Guilherme Ramos Castelo

Bachelor in Micro and Nanotechnologies Engineering

Ambient-processed Low-cost Perovskite-based Photovoltaics

Dissertation to obtain the degree of

Master of Science in
Micro and Nanotechnologies Engineering

Adviser: Dr. Manuel J. Mendes, Assistant Professor, Faculty of Sciences and Technology – New University of Lisbon

Co-Adviser: Dr. Ugur Deneb Menda, Pos-Doc Fellow, Faculty of Sciences and Technology – New University of Lisbon

Examination Committee:

Chairperson: Dr. Rodrigo Ferrão de Paiva Martins
Raporteur: Dr. João Manuel Gregório Mascarenhas
Member: Dr. Manuel João de Moura Dias Mendes

October, 2019

FACULDADE DE CIÊNCIAS E TECNOLOGIA
UNIVERSIDADE NOVA DE LISBOA

Ambient-processed Low-cost Perovskite-based Photovoltaics

"*The past has no power over the present moment*." – **Eckhart Tolle**

Acknowledgements

Primeiramente quero agradecer ao Prof. Dr. Rodrigo Martins e à Prof. Dra. Elvira Fortunato por me garantirem todas as condições de trabalho para realizar a minha tese, graças às excelentes instalações e equipamento ao dispor de todos os estudantes de materiais e nanotecnologias, no CENIMAT e no CEMOP. Em especial atenção agradeço aos meus orientadores Prof. Manuel Mendes e Dra. Deneb Menda por me terem dado a oportunidade de investigar na área da energia solar, a qual me cativa bastante e que irá ter ainda mais importância na nossa sociedade nos próximos tempos. Quero também agradecer a toda a equipa do CENIMAT e do CEMOP pela ajuda prestada sempre que necessitei.

I want to give a special thanks to my co-adviser, Dra. Deneb Menda, for everything that has done for me during these months working on the laboratory, all the work and life advices, all the time explaining and helping me in the laboratory, all the e-beam depositions, for never giving up, for always trying to motivate me when the work was not going well and for always being a positive person.

Não posso deixar de agradecer aos meus camaradas do CENIMAT que me acompanharam nesta caminhada difícil, bem como aos amigos que fiz ao longo destes 5 anos magníficos e que sempre me apoiaram nas alturas mais difíceis, com os quais vivi momentos e histórias incríveis e memoráveis e com os quais espero vir a recordá-las ao longo da nossa vida, sempre com a mesma amizade, alegria e cumplicidade, tais como o Guilherme Ferreira, Luís Bettencourt , Renato Nora, Joan Concha, João Vieira, Mafalda Pina, Mariana Moniz, Inês Tavares, Joana Rodrigues, entre outros.

Por fim, não posso deixar de agradecer à minha família, principalmente à minha mãe, pai, avós e tia que sempre me motivaram e apoiaram nos momentos mais complicados da minha vida académica em que por vezes me sentia desanimado e sem esperanças, e também por sempre tentarem fazer de mim uma pessoa melhor através dos seus ensinamentos e carinho que sempre me deram ao longo de toda a vida.

Um grandíssimo obrigado a todos vós!

Abstract

Perovskite solar cells (PSC) are one of the most promising photovoltaic (PV) technologies due to their quick and simple production, as well as their exceptional optoelectronic properties. However, their high price compared to the commercialized Si-based solar cells and their low scalability are some drawbacks that must be overcome.

In this thesis, these drawbacks were surpassed by substituting the costly materials by low-cost alternatives. Instead of Spiro-OMeTAD [1] as the hole transport material (HTM), a much cheaper material, CuSCN was used [2]. Furthermore, all the fabrication processes were performed in air under ambient conditions, avoiding the high cost and scalability problems associated with the use of a glove box. Considering this philosophy of low-cost development of the PSCs, the active layer was composed by MAI and PbI_2 as the precursors, which were dissolved in γ-Butyrolactone (GBL), while maintaining the TiO_2 as the electron transport material (ETM). Incisive analysis of the individual layers of the solar cells were performed by many characterization tools such as spectrophotometry, XRD and SEM-EDS.

As a result of several optimizations, a solar cell with V_{OC}, J_{SC}, FF and PCE values of 0.86 V, 15.29 mA/cm^2, 0.64 and 8.48%, respectively was fabricated surpassing the previous efficiency record of 6.35% obtained in previous works [3].

Keywords: Perovskite Solar Cells, Low-Cost Photovoltaics, CuSCN, $MAPbI_3$, Spin-Coating

Resumo

Células solares de perovskita (PSC) são uma das mais promissoras tecnologias fotovoltaicas (PV) devido à sua produção rápida e simples, bem como às suas excecionais propriedades optoeletrônicas. No entanto, o seu elevado preço, comparativamente ao das células solares de silício comercializadas, e a sua baixa escalabilidade, são inconvenientes que devem ser ultrapassados.

Nesta tese, estes inconvenientes são ultrapassados através da substituição dos materiais mais caros por alternativas de baixo custo. Em vez de ser Spiro-Ometad [1] o material transportador de buracos (HTM), é utilizado um material muito mais barato, o CuSCN [2]. Para além disso, todos os processos de fabricação foram realizados em condições ambientais normais, evitando assim os custos e problemas de escalabilidade associados à utilização de uma "glove box". Considerando esta filosofia de desenvolvimento de células de perovskita com baixo custo, a camada ativa é composta por MAI e PbI_2 como percursores, que foram dissolvidos em γ-Butirolactona (GBL), mantendo-se o TiO_2 como o material transportador de eletrões (ETL). Uma análise incisiva de todas as camadas foi efetuada, usando diversas ferramentas de caracterização, como espectrofotometria, XRD ou SEM-EDS.

Como resultado de várias otimizações, foi obtida uma célula solar com PCE de 8.48%, com VOC de 0.86 V, JSC de 15.29 mA/cm^2 e FF de 0.64, superando assim o recorde de eficiência de 6,35% obtido nos trabalhos anteriores [3].

Palavras-chave: Células Solares de Perovskita, Dispositivos Fotovoltaicos de Baixo Custo, CuSCN, $MAPbI_3$, Spin-Coating

Contents

List of Figures

List of Tables

Symbols

µL – Microliter

a-Si - Amorphous Silicon

A - Amperes

Au – Gold

c-Si - Crystalline silicon

CdTe - Cadmium telluride

cm – Centimeter

CuSCN - Copper(I) Thiocyanate

HCl - Hydrogen chloride

Li - Lithium

mA - Miliampere

mg - Miligrame

min – Minute

mL - Milliliter

mm - Millimeter

N/m – Newton/metre

nm - Nanometer

ºC - Degrees Celsius

Pb - Lead

PbI_2 - Lead iodide

rpm - Rotations per minute

s - Seconds

TiO_2 - Titanium dioxide

V - Voltage

ZnO - Zinc oxide

λ - Wavelength

Ω - Ohms

Acronyms

ABX3 - $MAPbI_3$ or $CH3NH3PbI_3$ - Methylammonium Lead Iodide

c.TiO_2 - Compact titanium dioxide

CAS - Chemical Abstracts Service

CIGS - Copper indium gallium selenide

CIS - Copper Indium Selenide

DMF - N,N-dimethylformamide

DMSO - Dimethyl Sulfoxide

EDS - Energy Dispersive Spectroscopy

ETL - Electron transport layer

ETM - Electron transport material

EtOH - Absolute Ethanol

FF - Fill factor

FIB - Focused ion beam

FTO - Fluorine-doped Tin Oxide

GBL - Gamma-Butyrolactone

HTL - Hole transport layer

HTM - Hole transport material

I_{SC} - Short-Circuit Current

J_{SC} - Short-Circuit Current Density

Li-TFSI - Bis(trifluoromethane) sulfonimide – Lithium salt

MAI - Methylammonium Iodide

mp.TiO_2 - Mesoporous titanium dioxide

NIR - Near infrared

PCE - Power Conversion Efficiency

PSC - Perovskite solar cell

PV - Photovoltaic

R_S - Series resistance

R_{SH} - Shunt resistance

RT - Room temperature

SC - Solar cell

SEM - Scanning electron microscopy

Spiro-MeOTAD - 2,2’,7,7’-tetrakis(N,N-di-p-meth-oxyphenylamine)-9’,9’-spirobifluorene

TTIP - Titanium (IV) isopropoxide

UV-Vis - Ultraviolet-Visible

V_{OC} - Open-circuit voltage

XRD - X-ray diffraction

Motivation and Objectives

The exponential growth of our global society requires a sustainable and renewable energy source that can secure our energetic needs. Solar energy industry is the main candidate to achieve this objective, due to its low pollution and impact in the environment, as well as its "infinite" sustainability because it only requires an energy source that is abundant (in one hour, the surface of the Earth receives enough solar energy to sustain all the energetic necessities of the humanity for one year) and reliable, the sunlight. Besides electricity generation (photovoltaics), solar energy can be used to generate heat (solar thermal), to purify water, to power satellites and, also, to reduce the CO_2 emissions [4].

The harvesting of solar energy by photovoltaic (PV) technology has been improving rapidly over the last decades, and the most dominant type of solar cells on the market are the silicon-based ones. Although this type of cells has achieved power conversion efficiencies (PCE) over 26% [5], their fabrication process requires vacuum and high temperatures, which leads to high production costs, and their morphology does not allow an alteration of shape or transparency. Due to these drawbacks, there has been an increasing focus on thin film solar cells for as an alternative, because they exhibit potential to have higher efficiencies, require simpler and cheaper production methods and can be produced on flexible or semi-transparent substrates.

One of the most promising classes of thin film solar cells are the perovskite solar cells (PSCs), due to the rapid increasing of their PCE, their easier and cheaper production techniques, such as spin-coating, that do not require vacuum neither extremely high temperatures, as well as their amazing optoelectronic and morphological properties.

This thesis objective is to produce low-cost perovskite solar cells through simple and quick production techniques, while aiming to improve their performance and efficiencies, using TiO2 as the electron transport material (ETM), $MAPbI_3$ as the active layer material and CuSCN as the hole transport material (HTM). Special focus is given on the active (perovskite) layer parameters and characterization, due to its extreme importance on the quality of the cell, as well as on the hole transport layer (HTL) because it is the use of CuSCN, instead of the typically used Spiro-MeOTAD, as the hole transport material, that significantly reduces the fabrication costs of the cells. In order to achieve these objectives, several parameters of the layers were studied, using many characterization equipment, such as the X-ray diffraction (XRD), the scanning electron microscope (SEM), the UV-Vis-NIR spectrophotometer and the solar simulator. For the electron transport layer (ETL), it was tested the effect of planar and mesoporous architecture and Li+ doping on the performance of the cells. For the perovskite layer, it was studied the impact of some perovskite parameters, such as its solution concentration, the volume of solvent deposited, the annealing time and temperature, on the overall quality of the cells. Finally, for the HTL, it was studied the influence of the CuSCN solution concentration and volume deposited, on the performance and morphology of the cells.

1. Introduction

1.1. History of Solar Cells

Solar cells are widely used on today's society, where they play a vital role of ensuring the energetic sustainability of our world. They only require a source of photons that, hopefully, will never cease to exist, the Sun, contrary to the other traditional energy sources that require non-renewable resources, such as fossil fuels or uranium, to generate energy.

Solar cells tend to be assumed as being a recent technology, but they were invented 65 years ago (1954). The first solar cell was silicon based and it was created by Chapin, Fuller, and Pearson at Bell Laboratories in New Jersey [6]. This cell had an efficiency of 6% but, in just 6 years (1960), Hoffman Electronics were able to get the efficiency up to 14% [7]. Since those times, the solar energy industry has increased exponentially through the years and nowadays, it is possible to produce solar cells with efficiencies up to 47% [8].

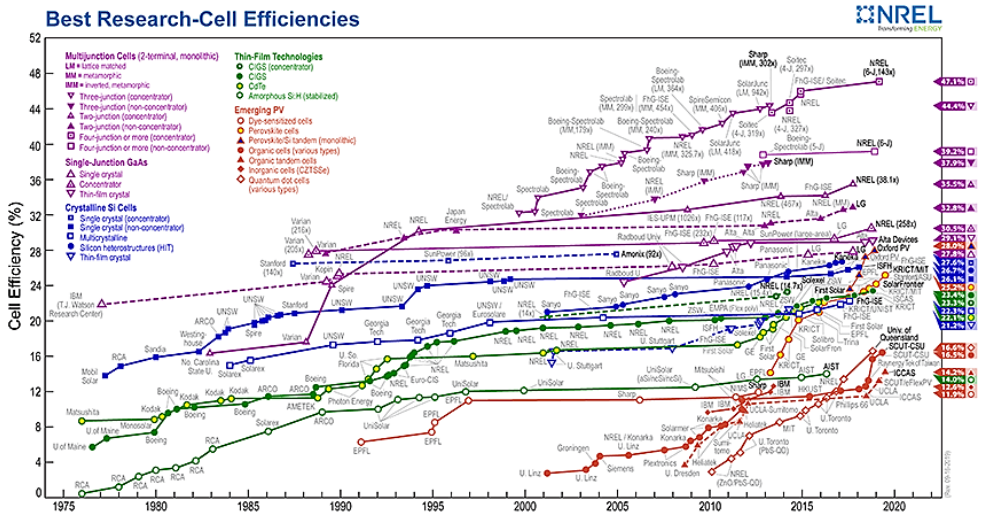

Figure 1 - Plot describing the best efficiencies obtained by all types of solar cells. (This plot is courtesy of the National Renewable Energy Laboratory, Golden, CO).

There are many types of solar cells and they are divided in three generations. The first generation cells are made by crystalline silicon wafers, they can be single crystal (higher efficiency) or multicrystalline (cheaper and easier production) solar cells. This generation still represents around 90% of the photovoltaic devices that currently exists worldwide [9]. The second generation consists of solar cells fabricated with thin film's materials, such as a-Si, CdTe, CIS and CIGS solar cells. They have lower efficiencies than the first generation cells but they are more visually pleasing, can be produced on larger areas and allow more applications on transparent and flexible substrates [10]. The third generation also consists of thin film technology but using organic, flexible and less toxic materials such as polymeric, dye sensitized, nanocrystal and perovskite solar cells [11].

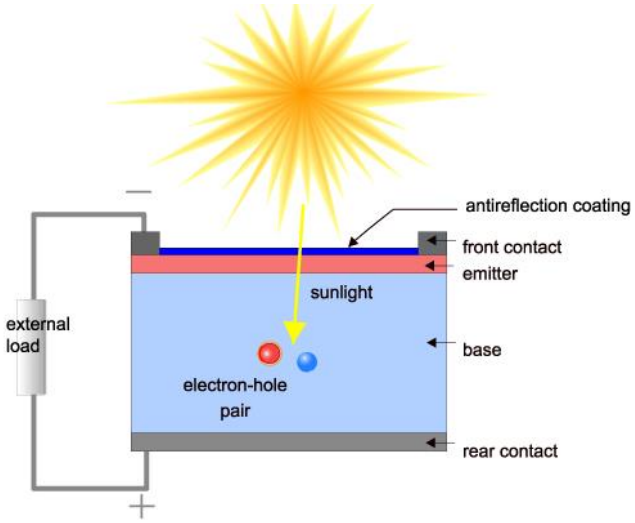

Figure 2 - Representation of the energy conversion process of a solar cell [12].

Perovskite solar cells (PSCs) are one of the most promising technologies to be a commercial alternative to the silicon solar cells. PSCs have low processing costs, are composed of abundant raw materials, produce low CO_2 emissions and have many remarkable possible applications like using them in building facades or in tandem perovskite–Si architecture as top cells [13]. Since their introduction in 2009, when the higher obtained efficiencies were around 3.8%, this technology witnessed an astonishing evolution and now (2019) the record efficiencies have reached over 25% [14],[15],[16]. Perovskite solar cells (PSCs) have been improving considerably, not only in terms of power conversion efficiency (PCE) but also regarding the device metrics such as the short-circuit current densities (J_{SC}), that have been reaching high values, as well as the fill factor (FF) and their corresponding open-circuit voltages (V_{OC}) values [17]. Therefore, to improve the PSCs efficiencies even more it is necessary to further increase the V_{OC} and FF values by reducing or eliminating any recombination pathways that might occur in the cell [18]. It is also vital for practical application to reduce the cells' production costs, increase their short lifetime, increase their efficiencies on flexible substrates and try to reduce their toxicity (e.g. due to presence of Lead, Pb), although it is lower compared to the Si technology [19].

1.2.1 Perovskite Properties

Perovskite materials follow the general formula ABX_3 and adopt a crystal structure arrangement where the 'A' and 'B' are cations (A is monocation, bigger than the dication B) that coordinate with the ´X´ anion. Normally, A is an organic molecule, such as FA or MA, B is either Sn or Pb and X is a halogen, like I, Cl, Br, or a combination of them. Since it is possible to adjust the material properties by mixing the different integrating elements it is common to achieve different variations of the organometal halide $CH_3NH_3BX_3$ that can form cuboctahedral and octahedral geometries, whose properties were first described by Weber in 1978 [20], [21], [22], [23]. These perovskite compounds have excellent properties for PV applications such as: (a) strong optical absorption of the visible and near-infrared spectra due to s-p antiboding coupling; (b) low surface recombination rate; (c) harmless grain boundary effects; (d) high electron and hole mobilities and diffusion lengths; (e) high tolerance to structural and shallow

point defects; (f) adjustable band-gap; (g) high carrier mobility and lifetime; (h) solution processability [20], [23], [24], [25]. They also exhibit different electronic properties, depending on the specific type of perovskite material, such as superconductivity, piezoelectric, semiconductivity and thermoelectric properties [25], [26], [27].

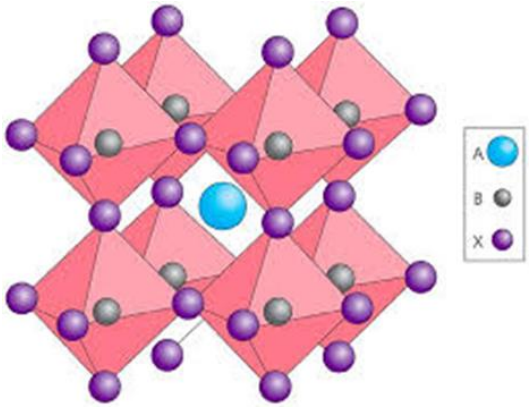

Figure 3 - Crystal structure of perovskites with the generic ABX3 configuration [25].

Although the perovskite materials have many beneficial properties, they also have some negative aspects like their toxicity caused by the lead, the photocurrent hysteresis observed in current density−voltage (J−V) curves of the cells, poor stability when exposed to high temperatures and illumination and, most importantly, their sensitivity to humidity and moisture which limits, considerably, the lifetime and overall quality of the cells [28]. This occurs because the MA cation is connected to the lead and iodide, by weak hydrogen bonds, which are easily broken or decomposed by water molecules [29]. To avoid these problems, the PSCs are normally fabricated in a glove box, or other highly controlled environment, that can regulate and maintain optimal atmospheric conditions, to enhance the performance and durability of the solar cells. Producing high efficiency PSCs without using these expensive equipment and controlled environments is a remarkable achievement, that represents the reduction of the PSCs manufacturing and selling price [28].

1.2.2 Architecture and Configuration

A perovskite solar cell has a more complex structure compared to a typical solar cell (Figure 2), with some apparent differences in the configuration of its layers as it is an hetero-junction. Normally, PSCs are composed of the following 6 layers: a) Transparent substrate, most commonly a transparent conductive oxide (TCO) coated on glass; b) Semiconductor compact layer, normally made of TiO_2 (n-type material which forms a n-i junction that regulates the flow of the electrons), known as the electron transport layer (ETL); 3) Semiconductor mesoporous layer, that acts as a scaffold for the perovskite layer deposition, which limits the hysteresis effects and promotes the motion of the electrons to the compact layer, increasing the carrier-collection efficiency, even if the photon absorption length is higher than the diffusion length of the charge carrier; 4) Active perovskite layer, which absorbs the light and creates the charge separation that leads them to their electrodes; 5) Hole transport layer (HTL), that is composed of a p-type material that acts as an i-p junction that regulates the hole transport mechanism; 6) Metallic electrode contact, normally made of gold, that allows a good bonding with the other layers. The valence band of the HTL must be higher than the perovskite valence

band and the ETL conduction band must be lower than the perovskite conduction band, to achieve a more efficient charge extraction and movement [30], [31], [32], [33].

The conventional n-i-p mesoscopic perovskite solar cell architecture (Figure 3(a)) is not exclusive, there are other variations of this structure. One is the inverted structure (p-i-n), where the layers are deposited in the reverse order of the conventional architecture (n-i-p) (Figure 4(d)). Both of these architectures, n-i-p and p-i-n, can also function without the mesoporous layer, which results in, so called, planar structures (Figure 4(b) and Figure 4(c)). The main differences, that distinguish the mesoscopic from the planar structure, are that the latter eliminates the porous metal oxide framework, which causes the formation of two interfaces between the perovskite materials and the two layers (ETL and HTL) and the thickness of the ETL in both structures (ETL in a planar structure is much thinner compared to one in a mesoscopic structure) [34], [35], [36], [37].

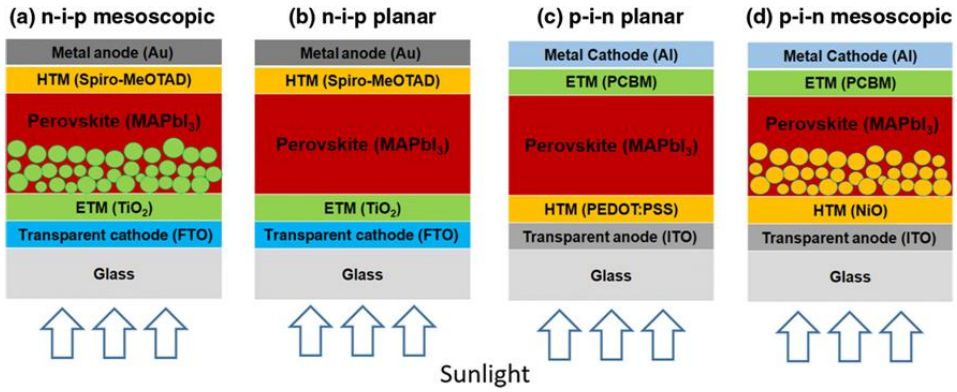

Figure 4 - Schematics of the most used configurations of a perovskite solar cell (PSC): a) n-i-p mesoscopic, b) n-i-p planar, c) p-i-n planar, d) p-i-n mesoscopic [33].

1.2.3 Device Preparation and Fabrication

After defining the configuration of the PSC, it is necessary to plan the composition and fabrication method of all the layers of the device. The most used deposition method is the spin-coating, when working with small-area (<10 cm^2) devices, because it is easy to operate, environmental friendly, cheaper and can achieve better film uniformity, compared to the other alternatives intended for large-area patterning like doctor blade coating, spray pyrolysis, dip-coating, inkjet printing, vacuum sublimation, thermal and chemical evaporation [38], [39], [40], [41], [42].

Firstly, the ETL, has the purpose of extracting and collecting electrons efficiently, so it must be composed of reliable semiconductor electron transport materials like SnO_2, ZnO or TiO_2. The most preferable material to be used as an ETL material, regardless if it is for a planar or mesoscopic ETL structure, is the TiO_2 due to its non-toxicity, chemical stability and favorable optical properties (transparent to the visible radiation, low absorption rate, high refractive index and high transmittance) [43], [44], [45]. These properties accompanied with the high electron transport length, increased electron injection rate, increased carrier lifetime, decreased electron-hole recombination rate and geometrical anti-reflection coating action created by the mesoporous material, makes TiO_2 a great ETL material [46], [47]. However, it also has a big disadvantage: it requires the formation of a compact ultra-thin layer that requires high annealing temperature (higher than 400 °C), which prevents the use of some cheap, light

and flexible substrates, due to their low melting temperatures, and also requires expensive heating equipment and energy costs [48].

Regarding the perovskite film, it is of extreme importance to optimize this layer in order to dramatically improve the overall quality and performance of the solar cell. This optimization of the perovskite layer can be done by controlling the parameters that influence its quality, crystallinity, energy level (Figure 5), and other morphological and functional properties, such as the deposition method, annealing time and temperature, atmospheric conditions and the perovskite solution processing method [26], [48]. There are many solvents to process the perovskite solution, such as N, N-dimethylformamide (DMF), Dimethyl Sulfoxide (DMSO) or γ-butyrolactone (GBL). The GBL is normally a better solvent for I-based perovskites due to its high solubility and necessity lower temperatures, while DMF and DMSO are most advised for the Br-based ones, although they also perform well as I-based perovskites solvents. DMF and DMSO strongly coordinate Pb2+, whereas GBL leads to the formation of clusters in the solution due to the weak interactions that occur between lead ions and the GBL molecules. When using DMF or GBL as solvents, the interaction of MAI with PbI_2 is slower, allowing a good crystallization of the $MAPbI_3$ crystals, when the solvents are evaporating [50], [51], [52].

The HTL, whose job is to selectively collect the holes and transport them to the metallic electrode, prevents the damage of the perovskite layer, by separating it from the metallic contacts and also minimizes the charge recombination that would happen on that interface (perovskite layer – metallic contacts) otherwise [50]. The most used HTL material in PSCs, according to the literature, and the one that achieves higher efficiencies is the Spiro-OMeTAD [41], [53]. However, this material has some drawbacks such as its high production cost [1], quick degradation with environmental conditions, low conductivity and hole mobility in its pristine form, and also causes self-aggregation when deposited [54]. One good alternative is the Copper(I) Thiocyanate (CuSCN), an inexpensive [2] and abundant metal halide of singly ionized copper that has a well-aligned work function, high hole mobility, good thermal stability, suitable energy levels and it is not easily degraded [55], [56], [57], [58].

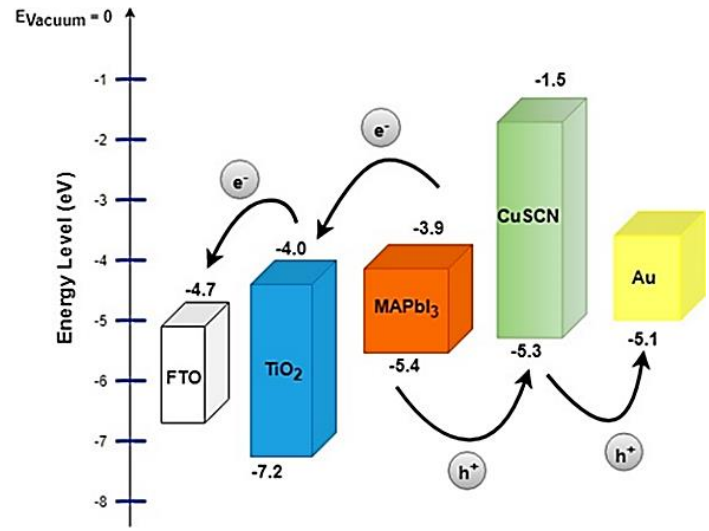

Figure 5 - Diagram of the energy level alignment of PSC layers used in this work (Based on [41]).

2. Methods and Materials

2.1. Device Fabrication

The solar cells' fabrication process consisted firstly by the etching of the fluorine-doped tin oxide (FTO) from the sides of the substrate, the cleaning of the glass substrates, the deposition of the electron transport layer (ETL), active layer (perovskite) and hole transport layer (HTL), and finally the gold contacts deposition. All the depositions, except the last one, were carried out via spin-coating (as presented in Figure 6) and the whole fabrication process was performed without a glove box, therefore there was no control or information of the temperature and moisture conditions. It is also important to refer that before each deposition, the unetched edges of the substrate were covered with kapton tape. Also, all the information regarding the reagents used in this work is presented in Table 11 from section B of Appendices.

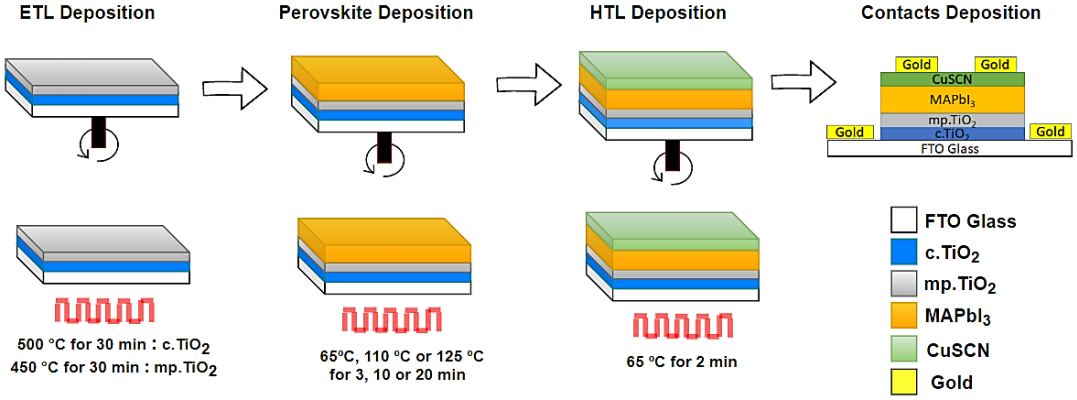

Figure 6 - Perovskite solar cell (PSC) layers deposition steps and corresponding annealing conditions. This work employed the conventional n-i-p superstrate configuration (Figure 4a).

2.1.1 Substrate Preparation and ETL deposition

The FTO coated glass substrates (100 mm x 100 mm x 2.2 mm, 13 Ω/sq, 82-84.5% of transmittance), cut into 2.5 cm x 2.5 cm, were etched with zinc powder, HCl + water solution and cotton buds. The substrates were then cleaned in an ultrasonic bath of detergent, ionized water (2 baths), acetone and ethanol, in this order for 15 minutes each, after which were dried with nitrogen flow and clean room paper and placed in the UV ozone system during 15 minutes for enhanced cleaning treatment. Regarding the ETL, it was firstly deposited the compact TiO_2 layer ($c.TiO_2$), whose solution is described in section C.1 of Appendices. 120 µL of the $c.TiO_2$ solution were dropped on the substrate and spun at 4000 rpm for 35 s with a ramp of 2000 rpm/s. The substrate was then dried at 120 °C for 10 minutes on the hot plate and then annealed in a furnace at 500°C for 30 minutes. After the substrate cools down, it is deposited the mesoporous TiO_2 ($mp.TiO_2$) layer, by dropping 120 µL of the $mp.TiO_2$ solution (described in Section C.1 of Appendices) on the substrate which is then spun at 4000 rpm with a ramp of 2000 rpm/s for 20 s and posteriorly dried for 10 min at 100 °C and annealed in the furnace for 30 min at 450 °C. It was also tested to perform a Li+ treatment of the $mp.TiO_2$ layer by depositing 150 µL, of LI-TFSI solution in acetonitrile (10mg/mL), at 3000 rpm with a ramp of 2000 rpm/s for 20 s, which was later annealed at 450 °C for more 30 min.

2.1.2 Perovskite Solution Preparation and Deposition

Before starting the perovskite layer deposition, the solutions (described in section C.2 of Appendices) were filtered through a 0.22 µm syringe filter and heated at 65 °C, as well as the substrate where it will be done the deposition. 100 µL of one of the solutions are then deposited and spin coated in a two-steps program at 1000 rpm for 10 s with a 500 rpm/s ramp and 5000 rpm, with a 2000 rpm/s ramp, for 20 s. When executing the second step, a certain volume (80 µL, 130 µL or 200 µL)) of toluene is poured on the substrate when there are 10 s left to the end of the program. After this process, the substrate is annealed at a defined temperature (65º, 110 °C, 125 °C) on the hot plate during a certain duration (3, 10 or 20 min).

2.1.3 HTL and Top Electrode Depositions

For the HTL, three solutions of copper(I) thiocyanate (CuSCN) powder dissolved in diethyl sulfide, with different concentrations (20 mg/mL, 35 mg/mL and 50 mg/mL) were filtered through a 0.22 µm syringe filter, and different volumes (35 µL, 50 µL or 80 µL) were deposited on the substrates by drop casting method, 2 seconds after the spinning program of 25 s at 3000 rpm with a 1000 rpm/s ramp started, and were then annealed at 65 °C for 2 min on the hot plate. Finally, the substrates are covered by acetate masks, produced by LASER (Universal LASER Systems) and the gold electrodes, with thicknesses around 100 nm and active areas dependent of the masks structure, are deposited by electron-beam evaporation under high vacuum, in a clean room.

2.2. Characterization

2.2.1 SEM-EDS

The top-surface and morphology images were obtained by Tabletop Microscope TM3030 Plus + Quantax 70 SEM and the cross-sectional images were examined by scanning electron microscopy (SEM) using a Carl Zeiss Auriga crossbeam (SEM-FIB) workstation instrument equipped with an Oxfotd Intruments Aztec X-ray energy dispersive spectrometer.

2.2.2 XRD

The crystal structures characterization of the substrates was done with X-ray diffraction (XRD) by using a PANalytical X'Pert Pro X-ray diffractometer in Bragg-Brentano geometry, with a monochromatic radiation source of Cu-Kα (λ=1.5406 Å).

2.2.3 UV-Vis-NIR Spectroscopy

The reflectance and total transmittance of all the samples were obtained by using a UV-Vis-NIR - Perkin Elmer Lambda 950 spectrophotometer with a ISR-260 integrating sphere within a wavelength range of 300-1200 nm.

2.2.4 Opto-electrical Characterization.

The I-V curves of the cells were measured by VeraSol-2 LED Class AAA Solar Simulator from Oriel, using forward scan (I_{SC} to V_{OC}) under ambient conditions at RT and with illumination intensity of one Sun (1 kW/m^2).

3. Results and Discussion

This chapter consists in the presentation and discussion of the results obtained from the characterization studies performed on the produced solar cells. The opto-electrical characterization was the most abundantly performed one, to assess the performance of the perovskite solar cells (PSCs), but other characterization tools were also employed for morphological, optical and structural analyses. The devices that were opto-electrically characterized were slightly different from those used for the other types of characterizations because, although being fabricated within the same conditions and having the same composition and structure, their rear side was coated with the gold electrode, thus preventing the cells to be used for some of the other measurements.

This chapter is divided into sections that analyse the influence of several parameters of the three main layers (electron transport layer, perovskite layer and hole transport layer) on the overall performance of a PSC with conventional n-i-p superstrate configuration (Figure 4a), giving special focus to the perovskite layer and the HTL. Through the study of these parameters, a PSC with an in-house record PCE (power conversion efficiency) was obtained, and its characterization and performance results are exhibited in this chapter, as well as a final study that regards the effect of time on the degradation of the PSCs.

3.1. ETL Layer Composition

This section correlates the composition of the ETL with the performance of the PSCs. Preferably, the ETL should have a high transmittance to facilitate the passage of light that goes through it, reaching the active layer more effectively. In Figure 7 b), it is possible to see that the transmittance of the substrate with mesoporous TiO_2 is higher than the one with only compact TiO_2 layer. This happens due to the mesoporous layer acting as a geometrical anti-reflective coating on top of the compact layer, which reduces its reflectance (as shown on the same figure) and enhances its transmittance, while maintaining its low absorbance, observed in Figure 7 a), as it is desirable for the ETL [59],[60]. The mesoporous layer also works as a photonic structure that minimizes the diffraction between the TiO_2 and the air, because its refractive index is lower than the one of the compact layer by itself (1.623 of the mp.TiO_2 vs 1.789 of the c.TiO_2) [61], which also contributes to the reduction of the total reflectance and corresponding increase of the total transmittance. Besides, the incorporation of the mesoporous TiO_2 also provides a wider surface-area connection between the ETL and the active layer, resulting in a more homogeneous and continuous flow of light that reaches the perovskite layer.

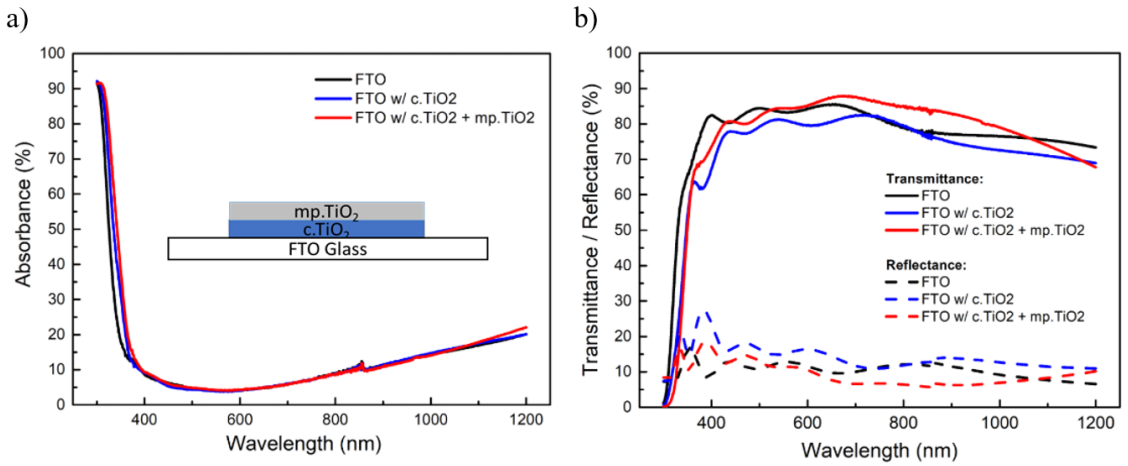

Figure 7 - a) Absorbance spectrum of only the ETL deposited over FTO, with only compact TiO2 layer (blue) and also with Mesoporous TiO2 over it (red), as well as the representation of the ETL architecture; b) Transmittance and Reflectance spectra of the same ETL.

An opto-electrical characterization of four cells with different ETL configurations was performed, with only a $c.TiO_2$ layer, with two $c.TiO_2$ layers, with the classic mesoscopic ETL ($c.TiO_2$ layer + $mp.TiO_2$ layer) and with the Li^+ doping ($c.TiO_2$ layer + $mp.TiO_2$ layer + Li-TFSI), because this last ETL composition achieved the best results in the latest M.Sc. work [3]. The results were extracted from the I-V curves which already exhibited the open circuit voltage (V_{OC}) and the short-circuit current density (J_{SC}) and, also, the equations presented in section A of Appendices were used to obtain the fill factor (FF), shunt resistance (R_{SH}), series resistance (R_S) and power conversion efficiency (PCE) of the cells. As can be seen, in Figure 8 and in Table 1, the cell that achieved the highest PCE value was the one who had a mesoscopic structure, whose ETL was composed only by a compact and mesoporous TiO_2 layer. This led to the conclusion that a mesoscopic ETL, without Li^+ treatment, is more reliable and achieves higher efficiencies so for all the following fabricated cells, analysed in this thesis, their ETLs were always deposited with this structure.

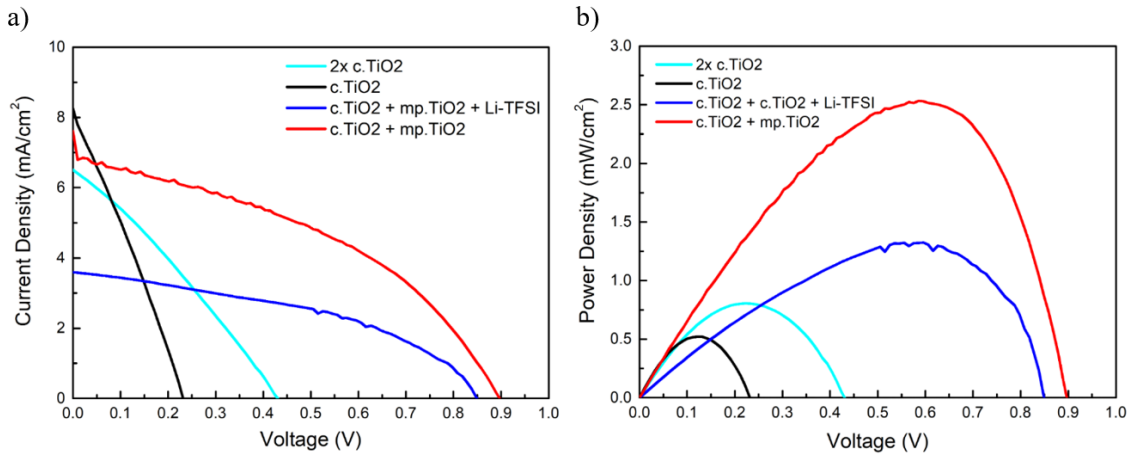

Figure 8 - a) J-V and b) P-V measurements of the four best solar cells with different ETL, which are composed of: 1x c.TiO2 (black), 2x c.TiO2 (cyan), c.TiO2 + mp.TiO2 (red) and c.TiO2 + mp.TiO2 + Li-TFSI (blue).

Table 1 – Electrical performance values (V_{OC}, Jsc, FF, R_{SH}, R_S and PCE) for the best devices (illustrated in Figure 8) obtained from a batch of 28 samples. The active area of the devices is 0.12 cm^2.

ETL Configuration	*V_{OC} (V)*	*Jsc (mA/cm^2)*	*FF*	*R_{SH} (Ω)*	*R_S (Ω)*	*PCE (%)*
1 c.TiO_2 layer	0.23	8.25	0.27	80.97	87.40	0.52
2 c.TiO_2 layers	0.43	6.51	0.29	822.62	390.98	0.81
c.TiO_2 + mp.TiO_2	0.90	6.86	0.41	2657.19	365.16	2.52
c.TiO_2 + mp.TiO_2 + Li-TFSI	0.68	3.60	0.43	6194.86	441.79	1.06

3.2. Perovskite Layer

The perovskite absorber layer is the one with most impact on the overall performance of the device, so, it is essential to obtain optimal conditions and quality for this layer. In this work, many studies regarding the perovskite layer were performed, many different perovskite solutions from the literature were prepared and tested, and several production parameters were compared and analysed. The perovskite solution that achieved the best results, on the initial trials, was the one described in Appendix C.2. Therefore, it was the solution used for all the studies presented in this thesis.

To analyse the influence of the production parameters on the quality of the perovskite layer, as well as on the overall performance of the devices, opto-electrical, optical, morphological and structural characterization were performed, and the results were considered. Due to this study, it was possible to verify a continuous improvement of the devices performance, as can be seen by the results and conclusions described along this section.

3.2.1 Effect of $MAPbI_3$ solution concentration

The perovskite solution concentration is a parameter that has not been studied much in the latest works, but it is a fundamental parameter to achieve a uniform perovskite layer with great quality. So, in this section, the effect of the $MAPbI_3$ solution concentration is deeply studied and it is observed the impact that it has on the performance of the devices.

Three solution concentrations (0.8 M, 1 M and 1.2 M) are investigated in this section, through the analysis of the optp-electrical, optical and structural characterization of different devices, which are composed by their respective solutions.

The optical spectra represented in Figure 9 show an unexpected result for the absorbance values of the devices. The 1.2 M perovskite concentration cell exhibits higher absorbance values, followed by the 0.8 M and the 1 M cells, by this order, which is contrary to what was expected, because as the concentration of the perovskite layer rises there should be a reduction of the light passing through the perovskite layer, which would decrease the transmittance values and increase the absorbance values. This is not verified in this case because the 0.8 M concentration sample exhibited higher absorbance values than the 1 M sample. Besides, as will be later described in this section, the cell that achieved a higher efficiency was the one with 1 M concentration. This incongruity can be explained by the fabrication and characterization procedure adopted in this work, where some cells with similar configurations

and composition, produced in identical conditions, were used only for the opto-electrical characterization, after the gold deposition, while the similar cells, without gold contacts, were used for the other characterization techniques (structural and optical). Even though the cells were produced in identical conditions, in perovskite technology it is quite difficult to achieve two exact twin cells, which explains these incongruities. Despite the differences between the absorbance values, the 1.2 M and 1 M samples have a similar band gap of 1.59 eV, while the 0.8 M has a lower band gap of 1.56 eV (values obtained by the Tauc plot represented in Figure 32 a) in section D of Appendices.

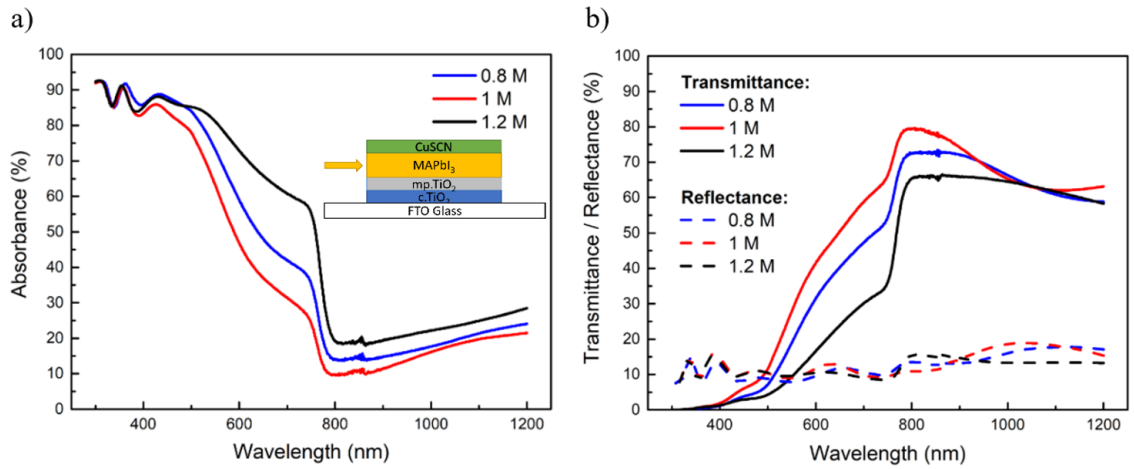

Figure 9 - a) Absorbance, b) Transmittance and reflectance spectra of three devices, which structure is illustrated on a), that are composed of perovskite layers that have different solution concentrations: 0.8 M (blue), 1 M (red) and 1.2 M (black).

The XRD results of the three devices (Figure 10) exhibit the (110), (112), (211), (202), (220), (310), (224) and (314) planes at an angle 2θ of 14.20º, 19.97º, 23.61º, 24.5º, 28.46º, 31.87º, 40.60º and 43.14º respectively, which denotes the presence of the tetragonal phase of the $MAPbI_3$, marked with full circle on Figure 10 [62], [63], [64], [65]. It is also noticeable the existence of the PbI_2 phase peak, due to its relatively low solubility in GBL, at an angle 2θ of 12.67º, the FTO diffraction peaks at an angle 2θ of 26.52º and 37.75º, and the CuSCN peak at an angle 2θ of 34.85º, that are pointed out, in Figure 10, with an open circle, asterisk and cardinal, respectively [66], [67], [68], [69]. Comparing the three XRD graphs, it is observed that the $MAPbI_3$ tetragonal phase peaks for the 0.8 M and 1.2 M are more intense than for the 1 M sample, which is a sign that these two substrates have a higher crystallinity in comparison to the 1 M. These results together with the absorbance spectrum presented in Figure 9 a), go along with the litterature, that relates higher crystallinity with higher absorbance values.

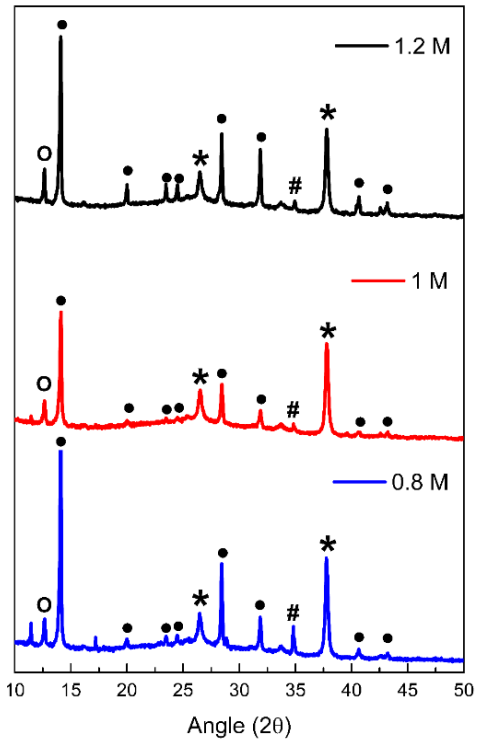

Figure 10 - XRD results of the samples (all layers deposited except gold) fabricated with different perovskite concentrations: 0.8 M (blue), 1 M (red) and 1.2 M (black). Tetragonal perovskite crystal structure peaks marked with full circle; PbI2 peaks marked with open circle; FTO peaks marked with asterisk; CuSCN peaks marked with cardinal.

The results obtained by the opto-electrical characterization measurements for this study are presented in Figure 11 by the J-V and P-V (power-voltage) curves extracted from the I-V curves of the PSCs. Table 2 describes all the electrical parameters of the PSCs, namely the open circuit voltage (V_{OC}), short circuit current density (J_{SC}), fill factor (FF), shunt resistance (R_{SH}), series resistance (R_S) and power conversion efficiency (PCE). By analysing these results, it is possible to observe a contradiction to the previous optical and structural analysis that pointed out the 1 M concentration substrate as having the lowest absorbance and crystallinity values. This is because the 1 M concentration cell achieved the best performance values, as can be seen by its PCE of 3.63%, which is more than 1% higher than that of the 1.2 M, and around two times higher than the one of the 0.8 M perovskite concentration. So, for all the following studies on this work, the 1 M perovskite solution concentration was used.

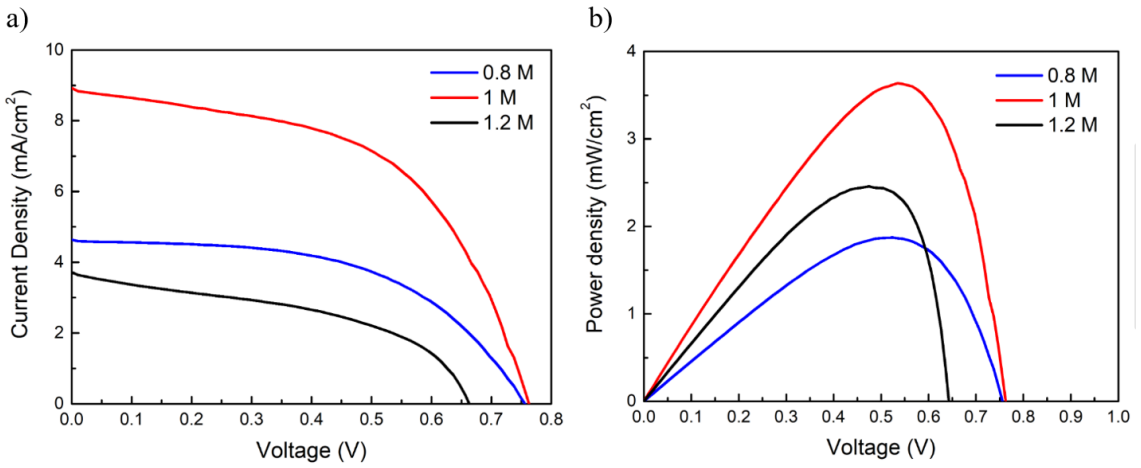

Figure 11 - a) J-V and b) P-V curves of the three best solar cells with different perovskite layer concentrations: 0.8 M (blue), 1M (red) and 1.2 M (black).

Table 2 – Electrical performance values for the best devices (illustrated in Figure 11) obtained from a batch of 40 samples. The active area of the devices is 0.12 cm^2.

Concentration	*V_{OC} (V)*	*Jsc (mA/cm^2)*	*FF*	*R_{SH} (Ω)*	*R_S (Ω)*	*PCE (%)*
0.8 M	*0.75*	*4.61*	*0.54*	*25167.21*	*472.91*	*1.87*
1 M	*0.76*	*8.87*	*0.54*	*5217.17*	*241.02*	*3.63*
1.2 M	*0.64*	*3.72*	*0.56*	*6381.78*	*96.15*	*2.45*

3.2.2 Effect of the toluene (anti-solvent) volume

The toluene deposition during the spinning of the perovskite solution is a necessary step to ensure the washing of the GBL (perovskite solution solvent), that has a high boiling point (204 ºC) which makes it impossible to evaporate during the annealing process [70]. This technique is an effective way to achieve uniform crystallization, controlled morphology and high reproducibility of the perovskite solar cells. The most important parameter for tuning is the amount of washing solvent deposited, because it affects the particle size distribution of the perovskite which has a great influence in the interconnections between the crystal grains [71]. Therefore, taking into account that all the samples have an area of 2.5 cm x 2.5 cm and the perovskite solution volume deposited is always 100 µL, the effect of the volume of anti-solvent deposited, during the perovskite layer spin-coating procedure, was tested by drop-casting three chosen volumes of toluene (80 µL, 130 µL and 200 µL - adequate for samples with these characteristics) and then analysing the results of opto-electrical, morphological and optical characterizations of the produced devices.

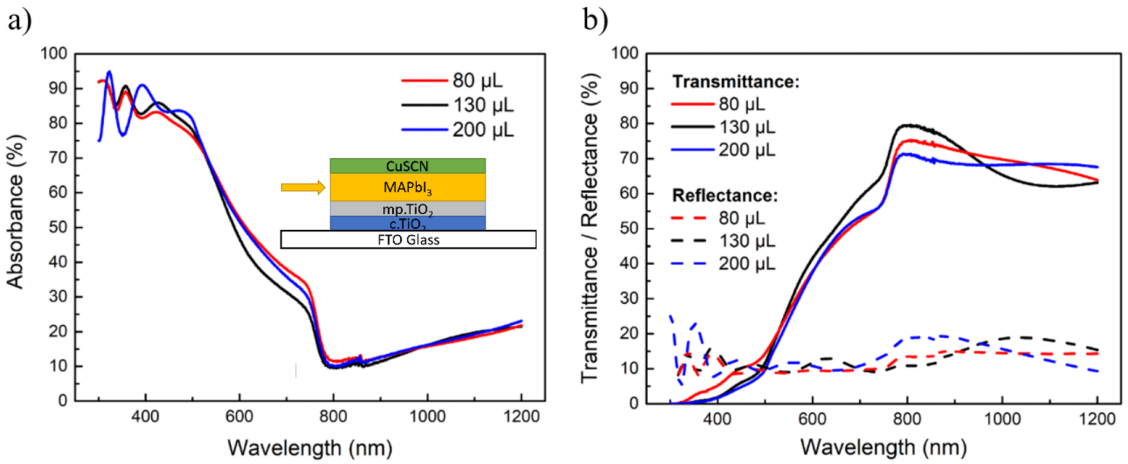

Figure 12 - a) Absorbance, b) Transmittance and reflectance spectra of three samples, whose structures are illustrated in the inset in a), that are composed of perovskite layers that were washed by toluene volumes of: 80 µL (red), 130 µL (black) and 200 µL (blue).

The three volumes of toluene resulted in cells with similar band gaps of 1.59 eV (value obtained by the Tauc plot represented in Figure 32 b) from section D of Appendices, and with close absorbance values , for the 80 µL and 200 µL that are relatively higher in comparison with the 130 µL ones, as shown in Figure 12 a). These results can be compared with the opto-electrical characterization results, presented in Figure 14 and summarized in Table 3, where we observe that the highest efficiency (PCE) corresponds to the 80 uL sample, which also has the highest absorbance value, followed by the 200 uL and the 130 uL, by this order. This leads to the conclusion that volumes of toluene deposition around 80 µL provide high absorption values which seem to be linked with better performances of the cells.

The influence of the volume of toluene deposited was also examined by the top-view SEM images represented in Figure 13, where it is possible to observe perovskite crystal structures with irregular shapes (some resembling a flower-like morphology), rough edges and high porosity that sometimes happen for perovskite solutions containing GBL as solvent [72]. It is also noticeable that the deposition of higher volumes of toluene seems to result in a wider disconnection of these crystals, creating larger gaps between them due to the washing of higher amounts of solvent, which contributes to the deagglomeration of the perovskite crystal structure resulting in a larger uncovered area beneath it [73].

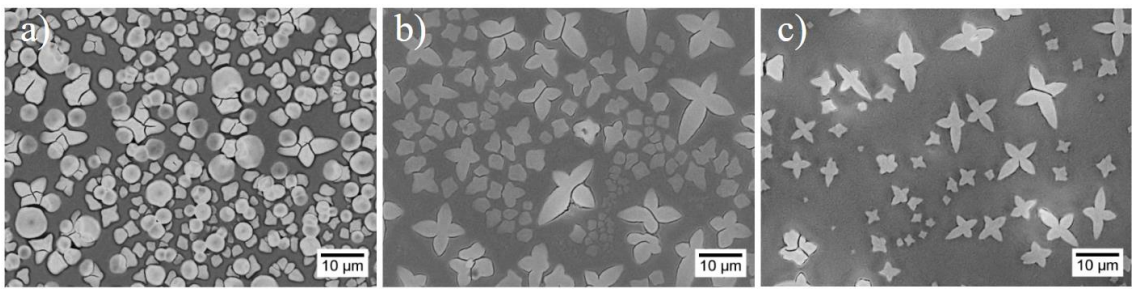

Figure 13 - Top-view SEM images of cells with perovskite layers washed by different toluene volumes: a) 80 µL, b) 130 µL, c) 200 µL. The samples are composed of all the layers with the exception of the gold contacts.

The results obtained by the opto-electrical characterization measurements for this study are presented in Figure 14 and in Table 3. In Figure 14 it is shown the J-V and P-V curves extracted from the I-V curves of the best contacts of the PSCs produced with different toluene washing volumes. Comparing the performance values of the three cells presented in Table 3, it is noticeable that the best cell is the one where 80 µL of toluene were dropped. This cell exhibits a V_{OC} of 0.79 V, J_{SC} of 11.32 mA/cm^2, FF of 0.52, and PCE of 4.64%, which is relatively higher than the other cells. Although the FF value is higher for the 200 µL cell, the 80 µL has a much higher J_{SC} and has the best PCE of the three. Therefore, as a result of this study, it is admitted that a toluene volume of 80 µL is ideal for better performances and electrical properties of the PSCs. As such, all the following studies on this work were performed using 80 µL of toluene as the chosen anti-solvent volume.

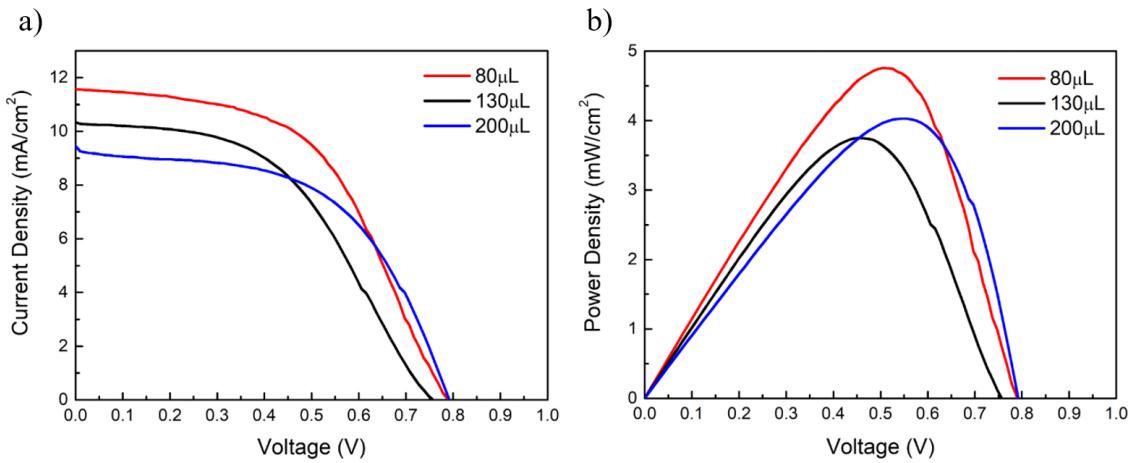

Figure 14 - a) J-V and b) P-V curves of the three best solar cells with different volumes of toluene washing deposited: 80 µL (red), 130 µL (black) and 200 µL (blue).

Table 3 - Electrical performance values for the best devices (illustrated in Figure 14) obtained from a batch of 30 samples. The active area of the devices is 0.12 cm^2.

Toluene Volume	***V_{OC} (V)***	***Jsc (mA/cm^2)***	***FF***	***R_{SH} (Ω)***	***R_S (Ω)***	***PCE (%)***
80 µL	*0.79*	*11.32*	*0.52*	*2612.94*	*129.29*	*4.64*
130 µL	*0.76*	*10.31*	*0.48*	*3440.99*	*209.62*	*3.75*
200 µL	*0.79*	*9.26*	*0.55*	*2389.70*	*83.33*	*4.03*

3.2.3 Effect of the Annealing Temperature of the Perovskite Layer

An important factor that highly influences the quality of the perovskite layer and the performance results of its corresponding cell, is the annealing temperature. This fabrication parameter also has a big impact in the device morphology and optical properties, as it will be observed by the studies performed in this section. According to the literature, PSCs produced with higher annealing temperatures exhibit faster degradation and lower lifetime, while the ones annealed with temperatures below a certain threshold (around 54ºC), do not crystalize and remain with a yellow coloration [74]. So, the temperatures chosen to perform this study were 65ºC (it is the pre-heating temperature of the substrates and, also the stirring temperature of the perovskite solution), 110ºC, which according to the literature is the temperature that provides higher efficiencies for this kind of perovskite [75], and 125ºC, that is a relatively high temperature which might cause a decay of its device performance values.

In this study, as can be observed in the plots represented in Figure 15, the sample that obtained a higher absorbance was the one annealed at 110ºC, but its absorbance values do not differentiate much from the ones of the sample annealed at 125ºC. On the other hand, the sample annealed at 65ºC exhibited a much lower absorbance and much higher transmittance values than its competitors, which might be related to a weak crystallization of the perovskite layer, due to the low temperature, which causes the light to pass through it much more easily, which is undesirable for PSCs. Despite the existing disparity between the absorbance values of the samples, they all have the same band gap value of 1.59 eV, as shown in Figure 32 c) from section D of Appendices.

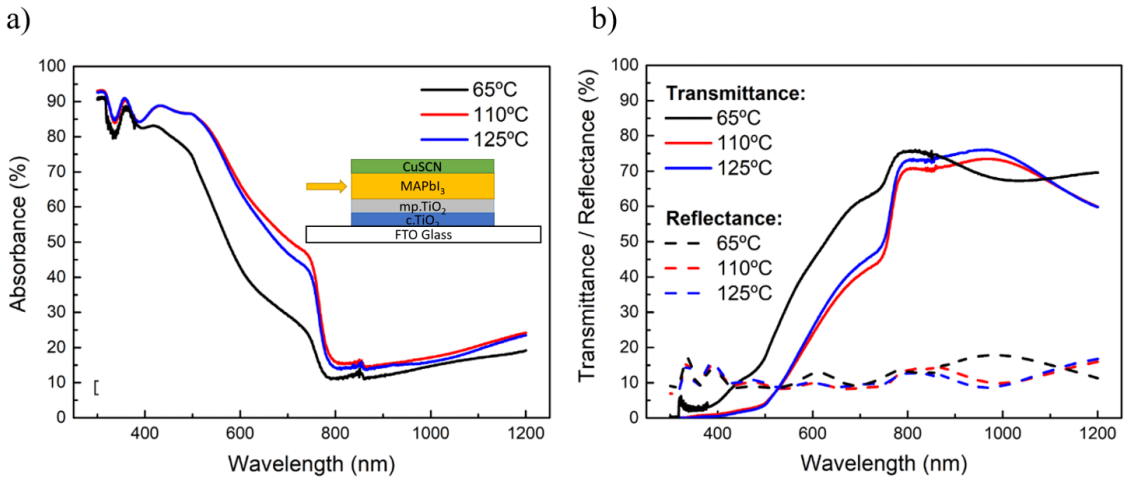

Figure 15 - a) Absorbance, b) Transmittance and reflectance spectra of three samples, which structures are illustrated on a), that are composed of perovskite layers annealed at a temperature of: 65ºC (black), 110ºC (red) and 125ºC (blue).

These three annealing temperatures also resulted in films with distinct surface morphologies, as can be seen in Figure 16. The SEM image of the sample annealed at 65ºC, Figure 16 a), reveals an inhomogeneous film with some zones where a full crystallization of the perovskite did not occur, probably due to the lack of enough temperature. For the annealing at 110ºC, Figure 16 b), a highly homogeneous film with regular grain size is visible, whereas for the sample annealed at 125ºC, Figure 16 c), its SEM image exhibits an irregular grain size and an inhomogeneous film with many vacancies, which might be indicative that the annealing

temperature used (125ºC) is close to the maximum threshold that the perovskite can sustain before starting to occur the degradation of its organic compound (MAI).

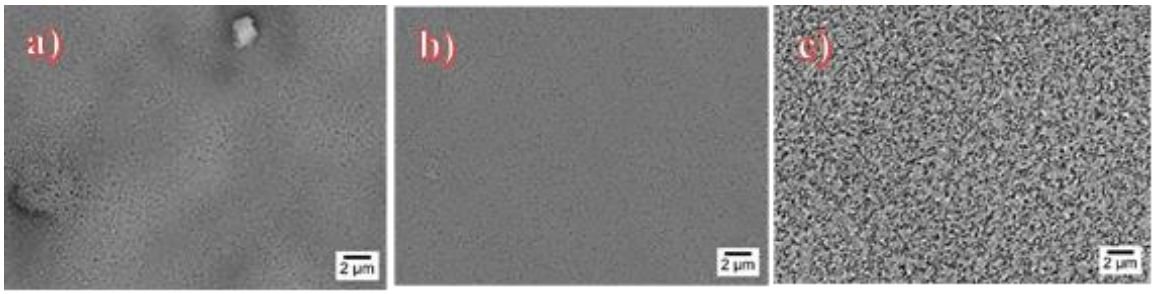

Figure 16 - Top-view SEM images of samples with different perovskite layer annealing temperatures: a) 65ºC, b) 110ºC, c) 125ºC . The annealing process of the perovskite layer had a duration of 10 minutes for all three samples. All the PSC layers were deposited on these samples with the exception of the gold contacts.

The J-V and P-V curves extracted from the opto-electrical characterization results of this study are shown in Figure 16 and the electrical parameters of the cells are described in Table 4. It is visible that the best cell of this batch, in terms of electrical performance, is the one that had its perovskite layer annealed at 110ºC, as can be seen by its PCE of 5.32%, V_{OC} of 0.70 V, J_{SC} of 11.84 mA/cm^2 and FF of 0.65. The PCE value is superior to the one obtained for the cell annealed at 125ºC (4.39%) and even more superior compared to the cell annealed at 65ºC (3.63%). Although there is a considerable difference of efficiencies, the cells have almost identical V_{OC} and FF values, which means that the parameter more affected by the annealing temperature was the J_{SC}. Besides, it is also concluded by the analysis of these results that it is more difficult to achieve PSCs with high electrical performance if the annealing temperature is low rather than higher temperatures (the PCE of the 125ºC cell is considerably higher than the 65ºC cell), which might be related to an incomplete crystallization of the perovskite layer.

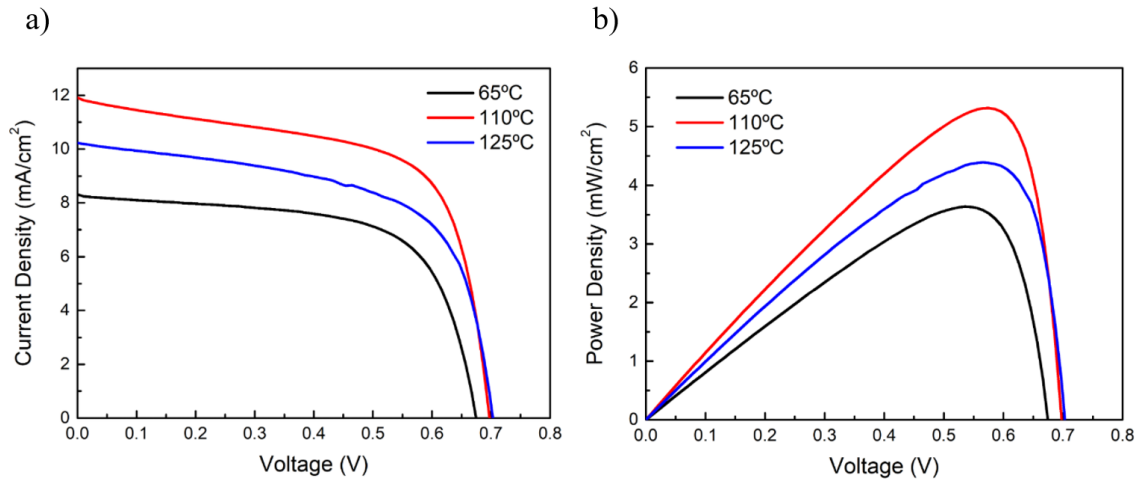

Figure 17 - a) J-V and b) P-V curves of the three best solar cells of which perovskite layer was annealed at different temperatures: 65ºC (black), 110ºC (red) and 125ºC (blue).

Table 4 - Electrical performance values for the best devices (illustrated in Figure 17) obtained from a batch of 30 samples. The active area of the devices is 0.12 cm^2.

Temperature	*V_{OC} (V)*	*Jsc (mA/cm^2)*	*FF*	*R_{SH} (Ω)*	*R_S (Ω)*	*PCE (%)*
65ºC	*0.68*	*8.26*	*0.65*	*5582.03*	*64.60*	*3.63*
110ºC	*0.70*	*11.84*	*0.65*	*3371.72*	*59.01*	*5.32*
125ºC	*0.70*	*10.21*	*0.61*	*2121.70*	*33.90*	*4.39*

3.2.4 Effect of the Annealing Time of the Perovskite Layer

According to the literature, the annealing time influences the crystallization and morphology of the perovskite films, and it is a interesting parameter to study because it provides information needed to optimize the production costs and time of the PSCs. It was chosen a short annealing time of 3 minutes to verify if it would be enough for the crystallization of the perovskite structure, an annealing time of 10 minutes that was considered the best one in many works that used this perovskite material ($MAPbI_3$) and also a longer annealing duration of 20 minutes to notice if it would start causing the degradation of the perovskite layer, due to overheating [76]. During the annealing step, it was not visible any difference at the naked eye between the cells annealed for 3 minutes and the ones annealed for 10 minutes because the crystallization of the perovskite layer was almost instantaneous (transition from a yellow to a brown coloration) but for the cell that was annealed for 20 minutes it was possible to observe a slight change of color to a more yellowish tone, on the last 2 minutes of annealing, that might be a signal of some degradation of the perovskite layer due to overheating.

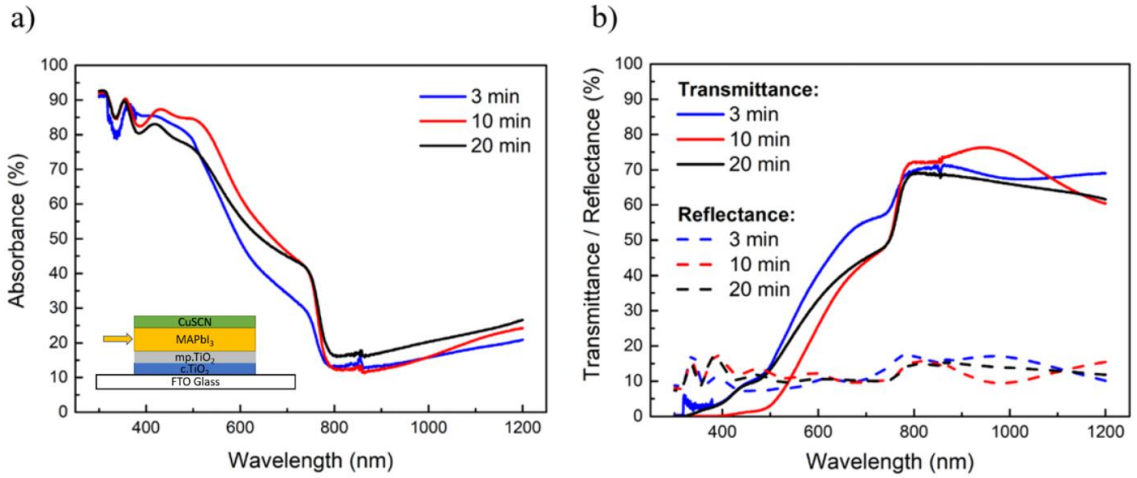

Figure 18 - a) Absorbance, b) Transmittance and reflectance spectra of three samples, which structures are illustrated on a), that are composed of perovskite layers annealed at a temperature of 110ºC during: 3 minutes (blue), 10 minutes (red) and 20 minutes (black).

An optical characterization study was performed and, as can be observed in the spectra represented in Figure 18, the sample that portrayed the best optical properties for a PSC (higher absorbance and low lower transmittance values) was the one annealed during 10 minutes, followed by the cell annealed for 20 minutes and the cell annealed during 3 minutes, by this order, which suggests that excessively short or long annealing times might not be advisable for the perovskite layer fabrication, as was referred before. Despite these differences on the optical

spectra, the cells annealed during 3 and 10 minutes obtained a similar band gap value of 1.59 eV whereas the cell annealed for 20 minutes presented a slightly lower band gap value of 1.58 eV, as in Figure 32 d) from section D of Appendices.

The results of the opto-electrical measurements are shown in Figure 19 and in Table 5, where it is possible to visualize the J-V and P-V curves extracted from the I-V results, and the values of the most important electrical parameters of the cells. The cell that exhibited the best performance values was annealed for 10 minutes, achieving a high PCE of 8.09%, a V_{OC} of 0.85 V, a J_{SC} of 14.75 mA/cm^2 and FF of 0.64. These values are much superior compared to the ones of its other two competitors, especially the V_{OC} value (0.14 V higher than the 20 minutes' cell and 0.16 V higher than the 3 minutes' cell), which is the main factor of such a disparity regarding the PCE values obtained. The cell that achieved the lowest PCE value, out of the three, was the cell annealed during 20 minutes, which is probably a result of overheating which might have triggered the decomposition of the perovskite crystal structure, lowering the stability of the cell as well as its lifetime. Therefore, as was expected and pointed out in the literature, the optimal annealing time to achieve better electrical performance values, for annealing temperatures close to 110ºC, is around the 10 minutes mark, because it is long enough to allow the crystallization of the perovskite layer but not to overheat the film which would cause the degradation of the perovskite crystal structure, and the reduction of the performance values of the cell.

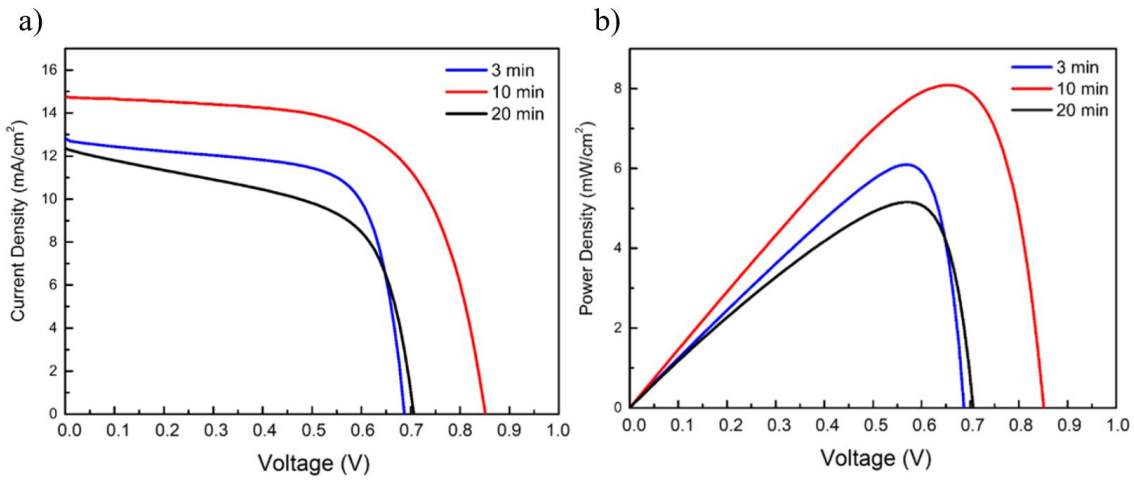

Figure 19 - a) J-V and b) P-V curves for the three best cells that had their perovskite layers annealed for different durations: 3 minutes (blue), 10 minutes (red) and 20 minutes (black).

Table 5 - Electrical performance values for the best devices (illustrated in Figure 19) obtained from a batch of 40 samples. The active area of the devices is 0.12 cm^2.

Duration	*V_{OC} (V)*	*Jsc (mA/cm^2)*	*FF*	*R_{SH} (Ω)*	*R_S (Ω)*	*PCE (%)*
3 min	*0.69*	*12.71*	*0.70*	*4849.93*	*56.17*	*6.10*
10 min	*0.85*	*14.75*	*0.64*	*6670.95*	*46.14*	*8.09*
20 min	*0.71*	*12.32*	*0.59*	*2450.85*	*67.98*	*5.16*

3.3. HTL CuSCN Parameters

The HTL is the layer responsible for the protection of the perovskite layer to prevent its quick degradation and, also has the function of "extracting" and transfer the holes from the perovskite layer, which requires a material with high hole mobility. Complementing these requirements with the philosophy of low-cost materials of this work, the choice for the HTM, as stated before, was the CuSCN which is a quite inexpensive and abundant p-type semiconductor with great thermal stability, high hole mobility and well-aligned work function [57]. Knowing the importance that this layer has on the overall performance of the PSC, it is fundamental that its fabrication parameters are studied and optimized. In this section the CuSCN solution concentration and the volume of solution deposited are studied through the analysis of the results obtained by the opto-electrical and optical characterizations performed. The CuSCN was always deposited above a perovskite layer fabricated according to the best parameters concluded in the previous section (concentration of 1 M, washed with 80 µL of toluene and annealed at 110ºC for 10 minutes). Also, the annealing parameters of the CuSCN layer were the same for all the produced cells, because on a study performed on a early stage of this work it was concluded that when the HTL was annealed for 2 minutes at 65ºC, the CuSCN was dried, had a good adherence to the substrate and did not deteriorate the perovskite layer, which resulted in cells with better electrical performances. The deposition method of the HTL was also tested, as seen in Figure 33 (from Section D of Appendices) and Figure 34 (from section E of Appendices), and it was concluded that the drop-casting technique, which consists in dropping the CuSCN solution during the spinning (2 to 5 seconds after spinning started), exhibits better optical and electrical performances than if the CuSCN solution is deposited before the spinning, so it was the adopted method for all the depositions of CuSCN during this work.

3.3.1 Effect of CuSCN Solution Concentration

The study described in this section regards the influence of the CuSCN solution concentration on the performance of the PSCs. The main focus of this study was on the analysis of the optical and opto-electrical characterization results, showcased in this section, to identify which of the three chosen CuSCN solution concentrations (20 mg/ml, 35 mg/ml and 50 mg/ml is the most appropriate one to achieve a PSC with high performance.

The results of the optical characterization are presented in Figure 20, where it is visible a great decrease of the absorbance values for the 20 mg/ml sample, which might be related to an insufficient thickness of the HTL due to the low concentration of CuSCN solution used. The other two concentrations used, exhibited more normal transmittance and absorbance values, with the 35 mg/ml sample having a slightly superior optical performance.

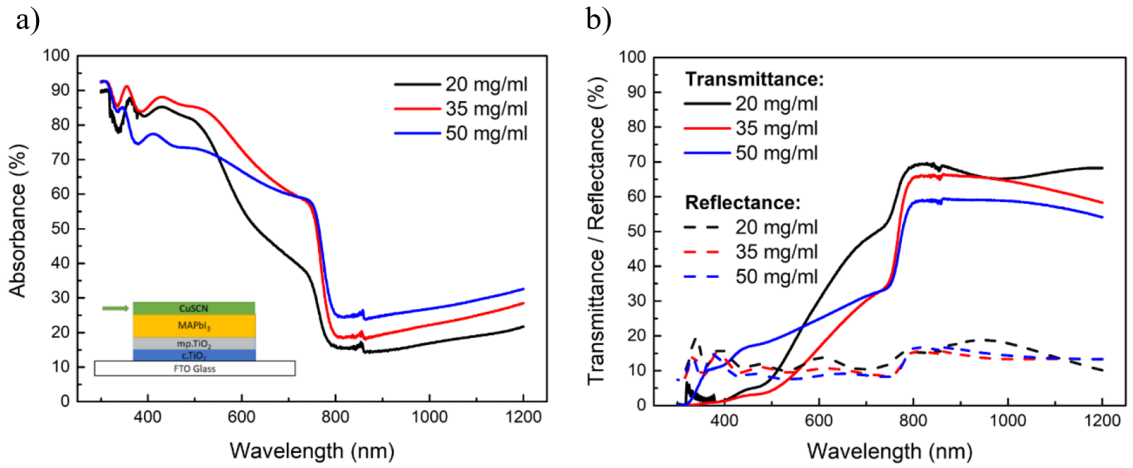

Figure 20 - a) Absorbance, b) Transmittance and reflectance spectra of three samples, which structures are illustrated on a), that possess HTLs with different CuSCN concentrations: 20 mg/ml (black), 35 mg/ml (red) and 50 mg/ml (blue).

From the opto-electrical characterization results the J-V and P-V curves of the cells produced with the three different CuSCN solution concentrations were extracted and are shown in Figure 21, with their respective electrical parameters being described in Table 6. As in the optical characterization, the 20 mg/ml cell also achieved lower results compared to the other two concentrations, as can be seen by its PCE that is less than half of the one obtained by the 35 mg/ml cell, which makes it, the worst choice of concentration for this specific PSC structure and composition. On the other hand, both the 35 mg/ml and 50 mg/ml cells revealed much better electrical performances, with the 35 mg/ml having a slightly superior PCE of 4.72% against 4.28 %, and also having higher V_{OC} and FF, while the 5 mg/ml achieved the highest J_{SC} out of the three, 10.59 mA/cm^2. In conclusion, according to the results obtained, for an HTL of PSC made with this specific layers and conditions, it is not advisable to use low concentrations of CuSCN nor too high concentrations, because as could be seen by the previous results even though the 50 mg/ml cell performance was close to the 35 mg/ml , there was already a decay in terms of absorbance and efficiency of the cell that might be related to excessive thickness of the HTL, which is unwanted, because the light that was not absorbed by the active layer needs to be transmitted through the HTL so it can be reflected by the gold contacts and be re-absorbed by the perovskite, and so, if the HTL is too thick, its transmittance will be reduced.

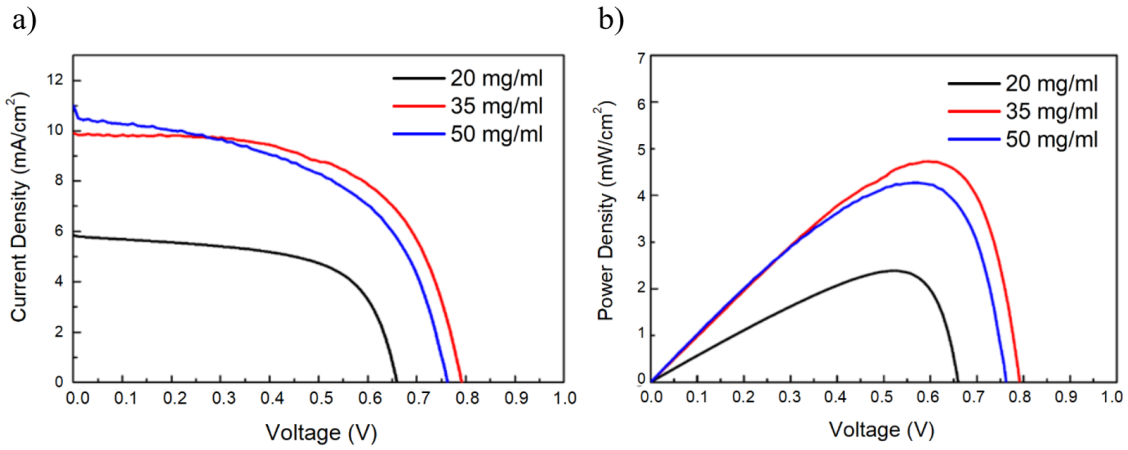

Figure 21 - a) J-V and b) P-V curves for the three best cells whose HTLs were fabricated with different CuSCN concentrations : 20 mg/ml (black), 35 mg/ml (red) and 50 mg/ml (blue).

Table 6 – Electrical performance values for the best devices (illustrated in Figure 21) obtained from a batch of 35 samples. The active area of the devices is 0.12 cm^2.

Concentration	*V_{OC} (V)*	*Jsc (mA/cm^2)*	*FF*	*R_{SH} (Ω)*	*R_S (Ω)*	*PCE (%)*
20 mg/ml	*0.6*	*5.81*	*0.62*	*6561.10*	*93.33*	*2.38*
35 mg/ml	*0.79*	*9.85*	*0.60*	*7032.18*	*81.11*	*4.72*
50 mg/ml	*0.76*	*10.59*	*0.53*	*4350.35*	*138.49*	*4.28*

3.3.2 Effect of CuSCN Volume Deposited

In this section, the volume of CuSCN solution deposited is studied, and its impact on the HTL quality and on the performance of the cell is evaluated. After searching and analyzing many studies of the literature [57],[67],[77], there seems to be no existing consensus regarding the optimal volume for the CuSCN deposition, although it is possible to verify that for smaller samples the highest volumes of CuSCN deposited (above 100 µL) normally lead to reduced performance values. Therefore, knowing that the devices were fabricated on small substrates with an area of 2.5 cm x 2.5 cm, the selected volumes of CuSCN for this study were 35 µL, 50 µL and 80 µL. As done for the previous studies, optical and opto-electrical characterizations were performed to decide which of the volumes provides more efficient cells.

The results of the optical characterization of the three devices are illustrated in Figure 22, where it is possible to observe similar absorbance and transmittance values for cells with 35 µL and 50 µL of CuSCN, while that the absorbance values obtained for the 80 µL were much more reduced, probably because the study about the deposition of this volume of CuSCN was performed on a different batch than the other two volumes.

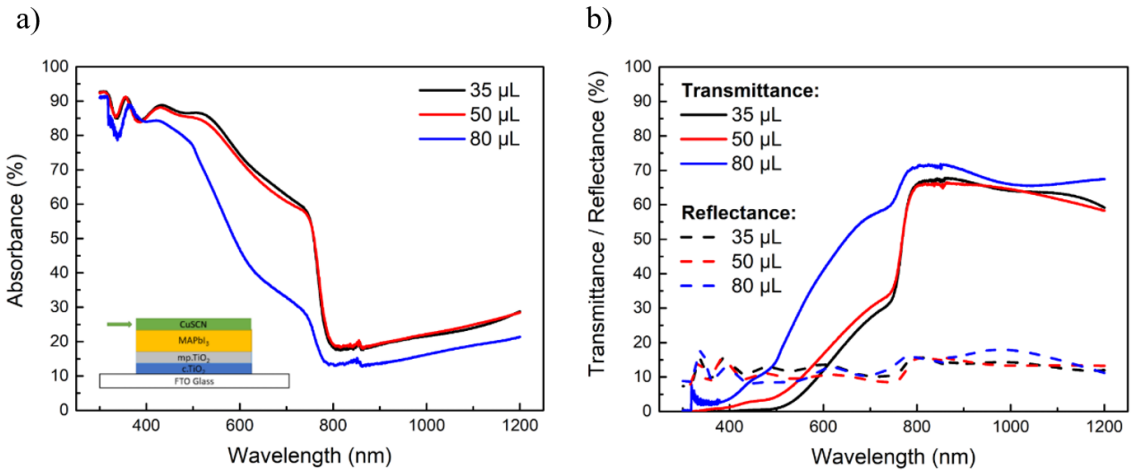

Figure 22 - a) Absorbance, b) Transmittance and reflectance spectra of three samples, with structures as illustrated on a), on which were deposited different volumes of CuSCN, with a concentration of 35 mg/ml, over their pervoskite layers: 35 µL (black), 50 µL (red) and 80 µL (blue).

The results of the opto-electrical characterization are illustrated as J-V and P-V curves in Figure 23 and the specific electrical values of the cells were extracted and summarized in Table 8. The cells obtained similar electrical efficiencies, which is usually an indicator that the parameter being study is not too relevant. Nevertheless, despite the values being close, there is still a cell that stands out from the others, the cell that had 50 µL of CuSCN deposited. This cell exhibited higher V_{OC}, J_{SC} and PCE values (0.71 V, 7.19 mA/cm^2 and 2.42%, respectively) but showed a lower FF than the other two cells (0.47 against 0.57 of 80 µL cell and 0.67 of the 35 µL cell). By observing these values, it is possible to conclude that this parameter (volume of CuSCN deposited) is the less relevant parameter studied until now, at least regarding the three volumes that were studied, because it did not seem to have a high influence on the overall performance of the cells.

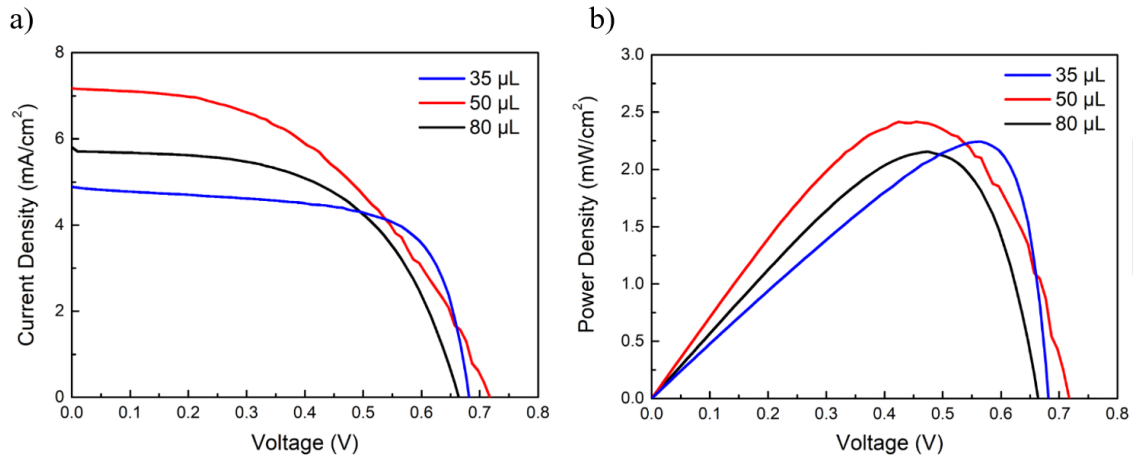

Figure 23 - a) J-V and b) P-V curves for the three best cells on which were deposited different volumes of CuSCN solution: 35 µL (blue), 50 µL (red) and 80 µL (black).

Table 7 – Electrical performance values for the best devices (illustrated in Figure 23) obtained from a batch of 25 samples. The active area of the devices is 0.12 cm^2.

Volume	*V_{OC} (V)*	*Jsc (mA/cm^2)*	*FF*	*R_{SH} (Ω)*	*R_S (Ω)*	*PCE (%)*
35 µL	*0.68*	*4.87*	*0.67*	*7260.72*	*64.49*	*2.24*
50 µL	*0.71*	*7.19*	*0.47*	*8816.29*	*236.88*	*2.42*
80 µL	*0.66*	*5.73*	*0.57*	*9196.90*	*262.58*	*2.15*

3.4. Best-performing Perovskite Solar Cell

According to all the analysis of the results performed in the previous sections of this work, it was concluded that the composition and manufacturing parameters of all PSC layers have a great influence on their electrical performance. Considering the "winners" of each of the parameters tested in this work, a PSC was designed with all these parameters that are described in Table 8, which resulted in the cell with the best electrical performance, obtained under uncontrolled environmental conditions and with low manufacturing costs. As can be seen from the J-V and P-V curves represented in Figure 24, as well as by observing the electrical performance values of this cell shown in Table 9, this is the cell that exhibited the best opto-electronic properties. The PCE value of 8.48 % obtained by this cell is noticeably high, given the conditions in which the cell was produced, as well as V_{OC}, J_{SC} and FF values of 0.86 V, 15.29 mA/cm^2 and 0.64, respectively, which leads to the belief that the selected properties and parameters, represented in Table 8, are the best suited ones to obtain PSCs with excellent electrical performance.

Table 8 - Composition and fabrication parameters of the best perovskite solar cell obtained.

ETL	Perovskite Concentration	Toluene Volume	Perovskite Annealing Temperature	Perovskite Annealing Time	CuSCN Concentration	CuSCN Volume
C.TiO_2 + Mp.TiO_2	***1 M***	***80 uL***	***110 ºC***	***10 min***	***0.35 mg/ml***	***50 uL***

Table 9 – Electrical performance values for the best performing PSC. Average PCE value obtained for this batch was 7.4% ± 1.1%. The active area of the device is 0.12 cm^2.

	V_{OC} (V)	*Jsc (mA/cm^2)*	*FF*	*R_{SH} (Ω)*	*R_S (Ω)*	*PCE (%)*
Best Cell	*0.86*	*15.29*	*0.64*	*7625.98*	*47.56*	*8.48*

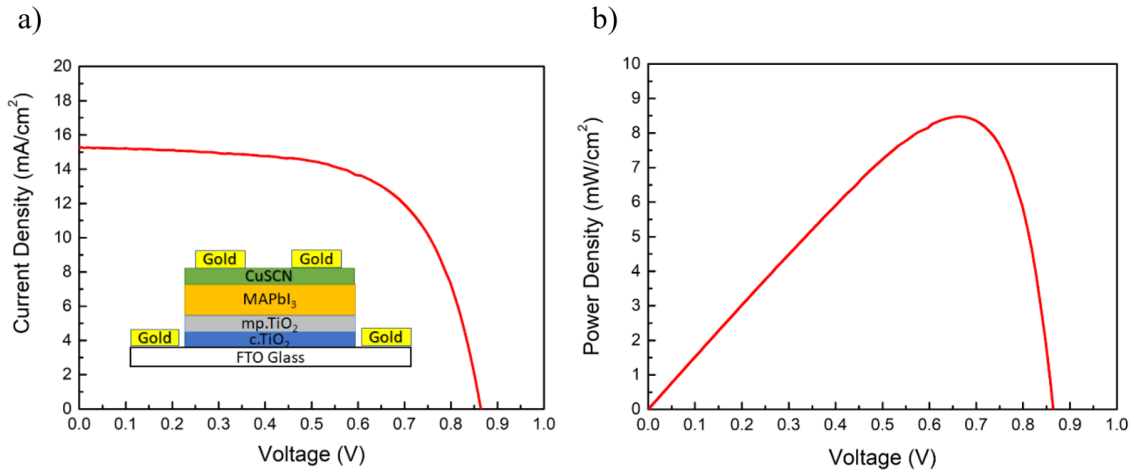

Figure 24 - a) J-V and b) P-V curves of the best perovskite solar cell obtained in this work. The structure of the complete cell is also illustrated in a).

Due to unavailability of some characterization equipment (SEM and SEM-FIB) at the time of production of the best cell, the optical and morphologic characterizations were performed for a cell produced with the exact same parameters and conditions although it had obtained a lower PCE of 6.10%.

An optical characterization study regarding the effect of the deposition of each layer, one by one, on the absorbance values of the device was performed, as shown in Figure 25 a). With the addition of each layer on the cell there is an increase of the absorbance values. However, with the addition of the the CuSCN layer, it is observed a slight decrease of the absorbance values of the cell after its deposition. This is merely attributed to the index-matching effect of this layer at the back of the cell rear, that slightly increases the transmission of the longer-wavelength light at the rear surface, which would not occur with the addition of the gold back contact layer to finalize the device.

It was also taken a top-view SEM image of the cell, shown in Figure 25 b), where it is revealed a film with good coverage, small grain size (around 200 nm) and some vacancies, quite similar to the ones obtained for almost all the cells of this work that were produced with this same recipe and fabrication parameters.

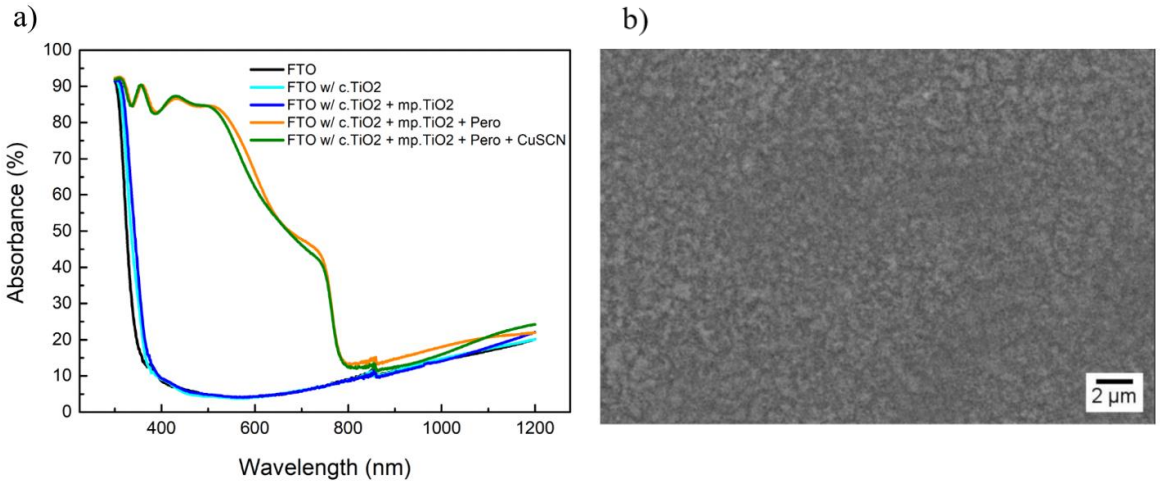

Figure 25 - a) Absorbance spectra obtained after each layer deposition, up until the HTL; b) Top-view SEM image of a cell obtained by the best fabrication parameters identified in Table 8.

An EDS characterization of the cell was also performed to verify the presence of the expected elements on each layer of the PSC. As can be seen in Figure 26, the elements of each layer are distributed as expected. It is also possible to observe in the same figure that the perovskite layer has a good thickness (around 300 nm), which is beneficial to provide high light absorbance in most of the sunlight spectral range. However, some holes in the perovskite layer are also visible (probably because this SEM-FIB cross-section image was not taken in the same week that the cell was produced), which is a negative factor because these holes act as "tunnels" for the light to pass through them, causing increased transmittance and reduced absorbance values.

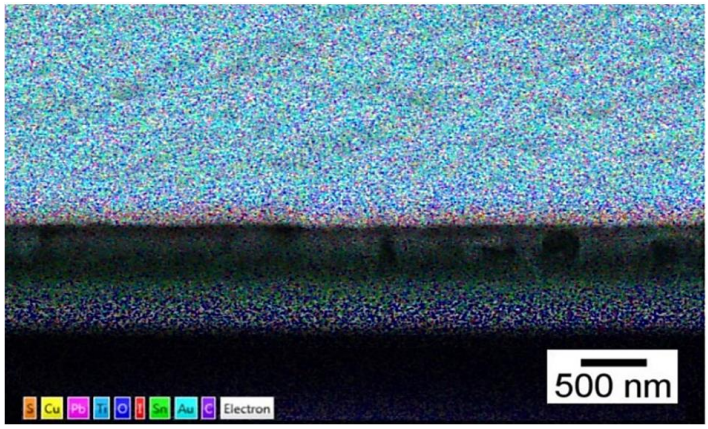

Figure 26 - SEM-FIB Cross section with EDS mapping of a PSC produced with the best fabrication parameters identified in Table 8.

3.5. Perovskite Solar Cells Degradation

The degradation of the PSC is one of the biggest problems of this technology that needs to be surpassed. Many things can cause the perovskite crystal to suffer degradation such as extended exposure to UV light, high temperature, humidity, prolonged exposure to oxygen, and also intrinsic factors like the vacancies that exist in the perovskite structure which can induce ion migration through the perovskite film leading to hysteresis effects and weak performances of the PSC. These factors can be minimized within an environment with controlled atmospheric conditions (e.g. glovebox). However, in this work there was little control over any of these parameters, the produced cells were left in closed boxes during the time frame that will be depicted in this section.

Here we studied the degradation upon exposure to ambient conditions of PSCs produced with the same composition and fabrication parameters of the best-performing cell simply by looking at their appearance with naked eyes (Figure 27), by imaging the morphology of its layers (Figure 28), and by measuring its electrical performance (Figure 29 and Table 10).

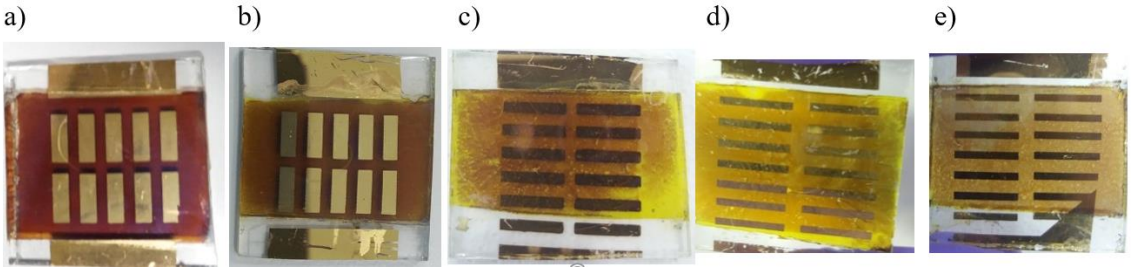

Figure 27 - Degradation stages of PSCs with similar composition: a) Day of fabrication; b) 1 day after; c) 1 week after; d) 1 month after; e) 2 months after.

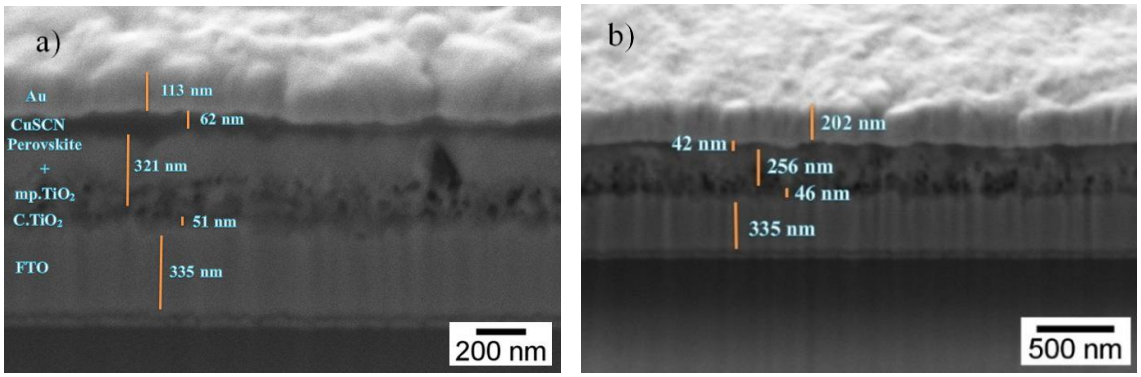

Figure 28 - SEM-FIB cross-section images of two different PSCs with similar compositions, taken at different times: a) 2 days after the cell's production; b) 2 months after the cell's production.

In Figure 27 it is possible to directly visualize the deterioration of the cells. As time passes by, they start losing their typical brown coloration, that is an indicator of the crystallization of the perovskite layer, and their coloration starts changing to a yellow colour after only 1 week of being exposed to ambient conditions (even though the cells were closed inside a box they are still affected by the ambient atmosphere) due to the formation of another phase of PbI_2.

The SEM-FIB cross-section image presented in Figure 28 b) reveals a quite significant reduction of the perovskite layer thickness in the 2 months' old cell (256 nm) compared to the image of the 2 days' old cell (321 nm), shown in Figure 28 a). It is also visible a slight difference in the thicknesses of the CuSCN and c.TiO_2 layers of each cell, which cannot be assured that is related to the time degradation because the studied cells are different and, so, even though they have the same composition and fabrication parameters, they are not exactly equal. Also, as the layers' thicknesses were all calculated through the ImageJ software, the observed difference lies within the expected margin of error.

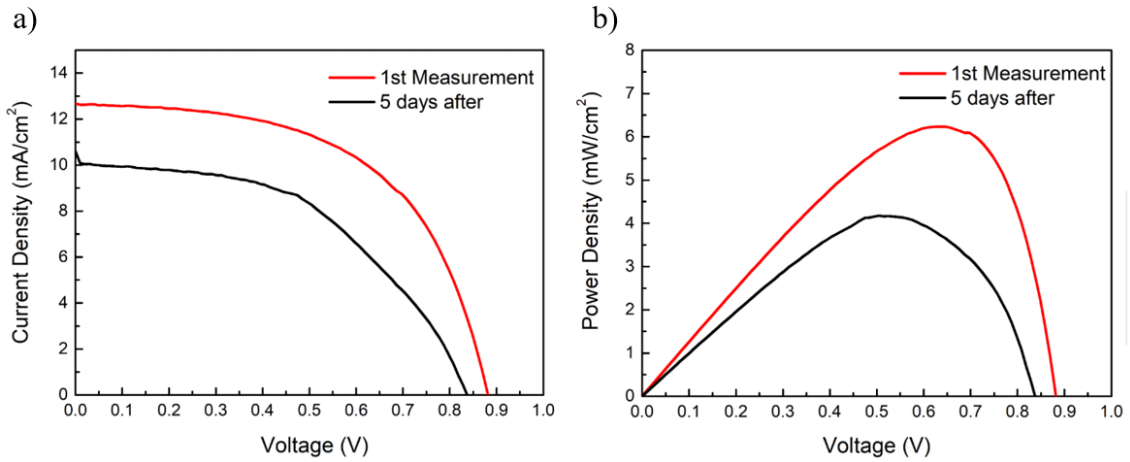

Figure 29 - a) J-V and b) P-V curves extracted from the opto-electrical characterization results of the same cell in two diferent days: Same day of production (red) and 5 days after production (black).

The IV characterization was performed to the same cell in the day that it was produced and five days later, to verify the effect of time on the electrical performance of the cell. As can be seen by the J-V and P-V in Figure 29, and by the values of the electrical parameters shown in Table 10, the cell exhibited a cutback on all its electrical parameters, the V_{OC} decreased 5%, the J_{SC} decreased 20%, the FF value had a 13% reduction and the PCE value declined 33% which is a significant reduction for measurements made only 5 days apart.

These results reveal that the bare PSCs have poor stability if they are left without encapsulation in ambient conditions, which demands for the implementation of effective encapsulants in future work.

Table 10 - Electrical performance values for the data illustrated in Figure 29. The active area of the device is 0.12 cm^2.

	V_{OC} (V)	Jsc (mA/cm^2)	FF	R_{SH} (Ω)	R_S (Ω)	PCE (%)
Same Day	*0.88*	*12.67*	*0.56*	*7735.93*	*98.17*	*6.23*
5 days after	*0.84*	*10.16*	*0.49*	*4128.20*	*168.15*	*4.18*

4. Conclusions and Future Perspectives

This work had the objective of producing perovskite solar cells at ambient air conditions, using low-cost reagents, as well as basic and fast production techniques, while also focusing on improving their electrical performance and optical properties. This was achieved through a continuous study of the layers of the PSCs, which were composed of TiO_2 as the electron transport layer (ETL) material, $MAPbI_3$ as the active layer material and CuSCN as the hole transport layer (HTL) material. This study focused more deeply on the active and hole transport layer's properties, and the optimization of their fabrication parameters. Nonetheless, some ETL configurations and materials were also tested to assure the best possible performance for the cells. In order to achieve valid conclusions about the parameters of the cells, many optical, morphological, structural and electrical characterizations were performed, and their results were systematically analysed and compared.

Firstly, the configuration and composition of the ETL were studied, and it was concluded that the best approach, for the specific properties of our perovskite solar cells, is to operate with a mesoscopic ETL composed of a compact TiO_2 and a mesoporous TiO_2 layer. This conclusion was taken from the analysis of the electrical characterization results which showed that the cell produced with a single compact TiO_2 layer plus a mesoporous TiO_2 layer exhibited a much higher PCE value (2.52%) compared to the cells that had only a compact TiO_2 layer (0.52%), or two compact TiO_2 layers (0.81%), or the ones which were doped with Li^+ (1.06%). It was also noticed an increase of the ETL transmittance values after depositing the mesoporous TiO_2 layer, which is beneficial because the absorption of this layer should be as low as possible to allow the transmittance of light through it, so that it can reach the perovskite absorber layer.

In the second section, four fabrication parameters and solution properties for the perovskite layer were studied and the best candidates of each parameter studied were picked. The tested parameters were the perovskite solution concentration, the volume of toluene deposited during the spinning, the annealing temperature and the annealing time of the perovskite layer. For the perovskite solution concentration, the cell that exhibited better electrical performance was the one that had perovskite with a concentration of 1 M, but the cells made with perovskite concentration of 0.8 M and 1.2 M achieved higher absorbance values. It was also visible that these two cells (0.8 M and 1.2 M) exhibited a higher crystallinity than the 1 M cell, but notwithstanding, all three cells revealed, on the XRD, the presence of the perovskite tetragonal phase of (110), (112), (211), (202), (220), (310), (224) and (314) planes at an angle 2θ of 14.20º, 19.97º, 23.61º, 24.5º, 28.46º, 31.87º, 40.60º and 43.14º respectively, and also revealed the presence of the PbI_2 phase at an angle 2θ of 12.67º, as well as the same FTO phase at an angle 2θ of 26.52º and 37.75º, and CuSCN peak at an angle 2θ of 34.85º. As the cell made with perovskite solution concentration of 1 M was the one that got the highest PCE out of the three (3.63% vs 1.87% of the 0.8 M cell and 2.45% of the 1.2 M) it was the selected concentration used for all the other studies. For the toluene volume study, it was concluded that the cell on which 80 μL were deposited achieved the best electrical performance and optical values, as compared to the 130 μL and 200 μL that were also tested. The annealing temperatures tested were 65ºC, 110ºC and 125ºC, and the conclusions taken from this study were that the cells annealed at 110ºC exhibit more homogeneous surfaces, better optical properties and higher electrical performances. So, the annealing temperature used for the other studies was always 110ºC, and the duration of the annealing selected was 10 minutes due to the electrical and

optical characterizations performed that revealed that a cell annealed for 10 minutes reaches higher absorbance values and PCE than if it annealed for a short time (3 minutes) or a long time (20 min).

The effects of changing the concentration and volume of the CuSCN solution were also tested. Through the analysis of the optical and electrical results it was concluded that the most adequate concentration of CuSCN for this type of cells is 35 mg/ml, and the quantity of CuSCN solution deposited should be around 50 ml.

It is also interesting to notice that for all of these studies the band gap values were all between 1.56 eV and 1.59 eV, which indicates that even though many different parameters were tested, the perovskites mantained similar band gap values.

The best cell was produced by using the winners of each parameter study and it achieved a PCE of 8.48%, which >2% higher than the best PCE (6.35%) reported in the previous works of the group performed with similar equipment and laboratory conditions [3]. This is an impressive result knowing that there was no control of the humidity or temperature, a glove box was not used, and the reagents used were low-cost compared to the ones used to fabricate the cells with highest efficiencies in the literature. Although the cell exhibited a great electrical performance it was also noticeable, from the degradation study performed, that the cells have low stability if left under ambient conditions which leads to the reduction of their efficiencies as time passes by.

4.1. Future Perspectives

As a future perspective, to achieve PSCs with higher electrical performance and higher stabilities it is vital that all the fabrication steps of the PSCs should be carried out inside a glove box, while also using a thermocouple on the hot-plate, to control the humidity and temperature conditions, that highly affect the quality of these cells. Also, a fine tuning of the parameters studied in this work should be done and it must be done a more profound structural characterization study throughout all the analysis of the parameters studied.

It should also be performed some investigation regarding the ETL, more specifically studying other materials such as Tin Oxide (SnO_2), Zinc Oxide (ZnO) or Cerium Oxide (CeO), for example, to test their effect on the quality of this layer and on the performance of the cells, as well as to explore the possibility of reducing the annealing temperature of the ETL, which would speed up and reduce the costs of the fabrication process. Besides, the reduction of the annealing temperature would also allow the fabrication of the PSCs on flexible substrates and even on paper substrates. Regarding the perovskite layer, it could be annealed using micro-wave annealing process [76], and also its composition could be altered to a lead-free perovskite, which would permit the reduction of the toxicity of the cells, that is a major drawback mainly caused by the lead iodide.

It would be interesting to test different configurations of the PSCs such as inverted structures or also the implementation of a new layer between the CuSCN layer and the gold contacts, which could be made of graphene oxide (GO) or IZO, for example, as cells containing these two materials have been achieving great electrical results recently, as well as enhanced stability and durability under full solar intensity exposure [78].

Finally, it would also be appealing to integrate these PSCs on tandem solar cells with different configurations, for instance on silicon-perovskite tandem cells, on perovskite/perovskite tandem cells with optimized band gaps or even on CIGS-perovskite tandem cells' structures.

Bibliography

[1] Spiro-MeOTAD price: https://www.sigmaaldrich.com/catalog/product/aldrich/792071 (Visited on 10/08/2019)

[2] CuSCN price: https://www.sigmaaldrich.com/catalog/product/aldrich/298212 (Visited on 10/08/2019)

[3] B. Esteves, "Perovskite solar cells: Optimization of Cost-Effective Production". Master thesis, Dep. of Materials Science, Univ. Nov. Lisboa, 2018.

[4] M.-E. Ragoussi and T. Torres. "New generation solar cells: concepts, trends and perspectives." In: Chem. Commun. 51 (2015), pp. 3957–3972.

[5] K. Yoshikawa, H. Kawasaki, W. Yoshida, T. Irie, K. Konishi, K. Nakano, T. Uto, D. Adachi, M. Kanematsu, H. Uzu, and K. Yamamoto. "Silicon heterojunction solar cell with interdigitated back contacts for a photoconversion efficiency over 26%." In: Nature Energy 2 (Mar. 2017), pp. 17032

[6] M. Chapin, D & S. Fuller, C & L. Pearson, G. A New Silicon p-n Junction Photocell for Converting Solar Radiation into Electrical Power. Journal of Applied Physics. 25. (1954), pp. 676-677.

[7] A. Goetzberger, J. Knobloch and B. Voss "Crystalline silicon solar cells", (1998), pp. 114-118.

[8] M. A. Green, E. D. Dunlop, D. H. Levi, J. Hohl-Ebinger, M. Yoshita, and A. W.Ho-Baillie. "Solar cell efficiency tables (version 54)." In: Progress in Photovoltaics:Research and Applications27.7 (2019), pp. 565–575

[9] P. G. V. Sampaio and M. O. A. González. "Photovoltaic solar energy: Conceptual framework." In: Renewable and Sustainable Energy Reviews 74.C (2017), pp. 590–601.

[10] M. Kibria, A.Ahammed, S.Sonyy, F.Sony and S.Hossain. "A Review: Comparative studies on different generation solar cells technology" (2014).

[11] H. Atwater and A. Polman, "Plasmonics for improved photovoltaic devices," Nat. Mater., vol. (2010), pp. 205–214.

[12] Solar cell structure: http://www.pveducation.org/pvcdrom/solar-cell-operation/solar-cell-structure (Visited on 11/08/2019)

[13] J.A. Christians, J.S. Manser, and P.V. Kamat. "Best practices in perovskite solar cell efficiency measurements. Avoiding the error of making bad cells look good." (2015), pp.852-857.

[14] A. Kojima, K. Teshima, Y. Shirai, and T. Miyasaka. “Organometal Halide Perovskites as Visible-Light Sensitizers for Photovoltaic Cells.” In: Journal of the American Chemical Society 131.17 (2009), pp. 6050–6051

[15] Z. Liu, P. You, C. Xie, G. Tang, and F. Yan. “Ultrathin and flexible perovskite solar cells with graphene transparent electrodes.” In: Nano Energy 28 (2016), pp. 151–157.

[16] Q. Tai, K.-C. Tang, and F. Yan. “Recent progress of inorganic perovskite solar cells.” In: Energy Environ. Sci.12 (2019), pp. 2375–2405.

[17] L. Qiu, O.K. Luis, and Q.Yabing. "Advances and challenges to the commercialization of organic–inorganic halide perovskite solar cell technology." Materials today energy 7 (2018), pp. 169-189.

[18] J. Wang, W. Fu, S. Jariwala, I. Sinha, A. K.-Y. Jen and D. S. Ginger. “Reducing Surface Recombination Velocities at the Electrical Contacts Will Improve Perovskite Photovoltaics.” In: ACS Energy Letters 4.1 (2019), pp. 222–227.

[19] Y. Rong, Y. Hu, A. Mei, H. Tan, M. I. Saidaminov, S. I. Seok, M. D. McGehee, E. H.Sargent, and H. Han. “Challenges for commercializing perovskite solar cells.” In: Science 361.6408 (2018).

[20] T.-B. Song, Q. Chen, H. Zhou, C. Jiang, H.-H. Wang, Y. (Michael) Yang, Y. Liu, J. You and Y. Yang. “Perovskite solar cells: film formation and properties.” In: J. Mater. Chem. A3 (2015), pp. 9032–9050.

[21] D. Weber. “CH3NH3PbX3, ein Pb (II)-system mit kubischer perowskitstruktur/CH3NH3PbX3, a Pb (II)-system with cubic perovskite structure.” In:Zeitschrift für Naturforschung B33.12 (1978), pp. 1443–1445.

[22] H. S. Jung and N.-G. Park. “Perovskite Solar Cells: From Materials to Devices.” In: Small 11.1 (2015), pp. 10–25.

[23] H. Snaith and M. Grätzel. “Electron and Hole Transport through Mesoporous TiO2Infiltrated with Spiro-MeOTAD.” In: Advanced Materials 19.21 (2007), pp. 3643–3647.

[24] J. Even, L. Pedesseau, and C. Katan "Theoretical insights into multi bandgap hybrid perovskites for photovoltaic applications", Proc. SPIE 9140, Photonics for Solar Energy Systems V, (2014).

[25] M. I. H. Ansari, A. Qurashi, and M. K. Nazeeruddin. “Frontiers, opportunities, and challenges in perovskite solar cells: A critical review.” In: Journal of Photochemistry And Photobiology C-Photochemistry Reviews 35 (2018), pp. 1–24.

[26] F. Sani, S. Shafie, H. Lim, and A. Ohinoyi Musa. “Advancement on Lead-Free Organic-Inorganic Halide Perovskite Solar Cells: A Review.” In: Materials 11 (2018), p. 1008.

[27] M. Xiao, F. Huang, W. Huang, Y. Dkhissi, Y. Zhu, J. Etheridge, A. Gray-Weale, U.Bach, Y.-B. Cheng, and L. Spiccia. “A Fast Deposition-Crystallization Procedurefor Highly Efficient Lead Iodide Perovskite Thin-Film Solar Cells.” In: AngewandteChemie International Edition 53.37 (2014), pp. 9898–9903.

[28] J. Troughton, K. Hooper, and T. M. Watson, “Humidity resistant fabrication of CH3NH3PbI3 perovskite solar cells and modules,” Nano Energy, vol. 39, (2017), pp. 60–68.

[29] S. N. Habisreutinger, D. P. McMeekin, H. J. Snaith, and R. J. Nicholas, “Research Update: Strategies for improving the stability of perovskite solar cells,” APL Mater., vol. 4, 2016.

[30] L. Wang, G. R. Li, Q. Zhao, and X. P. Gao, “Non-precious transition metals as counter electrode of perovskite solar cells,” Energy Storage Mater., vol. 7, (2017), pp. 40–47.

[31] J.-P. Correa-Baena, M. Saliba, T. Buonassisi, M. Grätzel, A. Abate, W. Tress, and A. Hagfeldt. “Promises and challenges of perovskite solar cells.” In: Science 358.6364 (2017), pp. 739–744.

[32] I. Mesquita, L. Andrade, and A. Mendes. “Perovskite solar cells: Materials, configurations and stability.” In: Renewable and Sustainable Energy Reviews 82.P3 (2018), pp. 2471–2489.

[33] M. Grätzel, “The light and shade of perovskite solar cells,” Nature. Mater., vol. 13, no. 9, (2014), pp. 838– 842.

[34] D. Zhou, T. Zhou, Y. Tian, X. Zhu, and Y. Tu. “Perovskite-based solar cells: materials, methods, and future perspectives.” In: Journal of Nanomaterials 2018 (2018).

[35] M. Abdi-Jalebi, M. I. Dar, A. Sadhanala, S. P. Senanayak, F. Giordano, S. M. Zakeeruddin, M. Grätzel, and R. H. Friend. “Impact of a Mesoporous Titania–Perovskite Interface on the Performance of Hybrid Organic–Inorganic Perovskite Solar Cells.” In: The Journal of Physical Chemistry Letters 7.16 (2016), pp. 3264–3269.

[36] M. A. Green, A. Ho-Baillie, and H. J. Snaith, “The emergence of perovskite solar cells,” Nat. Photonics, vol. 8, (2014), pp. 506–514.

[37] I. Hussain, H. P. Tran, J. Jaksik, J. Moore, N. Islam, and M. J. Uddin. “Functional materials, device architecture, and flexibility of perovskite solar cell.” In: Emergent Materials1.3-4 (2018), pp. 133–154.

[38] N. J. Jeon, J. H. Noh, Y. C. Kim, W. S. Yang, S. Ryu, and S. I. Seok. “Solvent engineering for high-performance inorganic–organic hybrid perovskite solar cells.” In: Nature Materials 13.9 (2014), pp. 897–903.

[39] J. Burschka, N. Pellet, S.-J. Moon, R. Humphry-Baker, P. Gao, M. K. Nazeeruddin, and M. Grätzel. “Sequential deposition as a route to high-performance perovskite- sensitized solar cells.” In: Nature 499.7458 (2013), pp. 316–319.

[40] A. T. Mallajosyula, K. Fernando, S. Bhatt, A. Singh, B. W. Alphenaar, J.-C. Blancon, W. Nie, G. Gupta, and A. D. Mohite. “Large-area hysteresis-free perovskite solar cells via temperature-controlled doctor blading under ambient environment.” In: Applied Materials Today 3 (2016), pp. 96–102.

[41] M. Ye, X. Hong, F. Zhang, and X. Liu, “Recent advancements in perovskite solar cells: flexibility, stability and large scale,” J. Mater. Chem. A, vol. 4, no. 18, (2016), pp. 6755–6771.

[42] X. Tong, F. Lin, J. Wu, and Z. M. Wang, “High performance perovskite solar cells,” Adv. Sci., vol. 3, no. 5, (2015), pp. 1–18.

[43] P. Gao, M. Gratzel, and M. K. Nazeeruddin, “Organohalide Lead Perovskites for Photovoltaic Applications,” Energy Environ. Sci., vol. 7, (2014), pp. 2448–2463.

[44] M. B. Karoui, Z Kaddachi, and R Gharbi. “Optical properties of nanostructured TiO2 thin films.” In: Journal of Physics: Conference Series 596 (2015), p. 012012.

[45] Y. M. Evtushenko, S. Romashkin, N. Trofimov, and T. Chekhlova. “Optical properties of TiO2 thin films.” In: Physics Procedia 73 (2015), pp. 100–107.

[46] M. Abdi-JalebiM., M. I. Dar, A. Sadhanala, S. Senanayak, F. Giordano, S.M. Zakeeruddin, and M.Gratzel (2016). “Impact of a Mesoporous Titania−Perovskite Interface on the Performance of Hybrid Organic−Inorganic Perovskite Solar Cells”. In: The Journal of Physical Chemistry Letters, 7, (2016), 3264-3269

[47] A. Marchioro, J. Teuscher, D. Friedrich, M. Kunst, R. Van De Krol, T. Moehl, M.Grätzel, and J.-E. Moser. “Unravelling the mechanism of photoinduced charge transfer processes in lead iodide perovskite solar cells.” In: Nature photonics 8.3 (2014), p. 250.

[48] S. S. Shin, W. S. Yang, J. H. Noh, J. H. Suk, N. J. Jeon, J. H. Park, J. S. Kim, W. M.Seong, and S. I. Seok. “High-performance flexible perovskite solar cells exploiting Zn2SnO4 prepared in solution below 100 C.” In: Nature communications 6 (2015), p. 7410.

[49] N.-G. Park, M. Grätzel, and M. Tsutomu. “Organic-Inorganic Halide Perovskite Photovoltaics”. In: Springer International Publishing, 2016, pp. 1–366.

[50] S. A. Fateev, A. A. Petrov, V. N. Khrustalev, P. V. Dorovatovskii, Y. V. Zubavichus,E. A. Goodilin, and A. B. Tarasov. “Solution Processing of Methylammonium Lead Iodide Perovskite from γ-Butyrolactone: Crystallization Mediated by Solvation Equilibrium.” In: Chemistry of Materials 30.15 (2018), pp. 5237–5244.

[51] B. Conings, J. Drijkoningen, N. Gauquelin, A. Babayigit, J. D'Haen, L. D'Olieslaeger,A. Ethirajan, J. Verbeeck, J. Manca and E. Mosconi. "Intrinsic thermal instability of methylammonium lead trihalide perovskite." In: Advanced Energy Materials 5.15 (2015), p. 1500477.

[52] M. Ye, C. He, J. Iocozzia, X. Liu, X. Cui, X. Meng, M. Rager, X. Hong, X. Liu, and Z. Lin. "Recent advances in interfacial engineering of perovskite solar cells." In: Journal of Applied Physics 50, (2017), p. 373002.

[53] G. A. Casas, M. A. Cappelletti, A. P. Cédola, B. M. Soucase, and E. L. Peltzer Blancá, "Analysis of the power conversion efficiency of perovskite solar cells with different materials as Hole-Transport Layer by numerical simulations," In: Superlattices Microconstruction vol. 107, (2017), pp. 136–143.

[54] Y. Hua, P. Liu, Y. Li, L. Sun, and L. Kloo. "Composite Hole-Transport Materials Based on a Metal-Organic Copper Complex and Spiro-OMeTAD for Efficient Perovskite Solar Cells." In: Solar RRL 2.5 (2018), p. 1700073.

[55] M.-H. Li, J.-H. Yum, S.-J. Moon, and P. Chen. "Inorganic p-type semiconductors: their applications and progress in dye-sensitized solar cells and perovskite solar cells." In: Energies 9.5 (2016), p. 331.

[56] Y. S. Lee, J. Heo, M. T. Winkler, S. C. Siah, S. B. Kim, R. G. Gordon, and T. Buonassisi."Nitrogen-doped cuprous oxide as a p-type hole-transporting layer in thin-film solar cells." In: J. Mater. Chem. A1 (2013), pp. 15416–15422.

[57] J. E. Jaffe, T. C. Kaspar, T.C. Droubay, T. Varga, M. E. Bowden and G. J. Exarhos. "Electronic and Defect Structures of CuSCN". In: J. Phys. Chem. C (2010) pp. 9111–9117.

[58] P. Vivo, J. K. Salunke, and A. Priimagi. "Hole-Transporting Materials for Printable Perovskite Solar Cells," In: Materials (Basel) vol. 10, (2017), pp. 1–45.

[59] S. Haque, M. J. Mendes, O. Sanchez-Sobrado, H. Águas, E. Fortunato, and R. Martins."Photonic-structured TiO2 for high-efficiency, flexible and stable Perovskite solar cells." In: Nano Energy 59 (2019), pp. 91 –101.

[60] M. J. Mendes, A. Araújo, A. Vicente, H. Águas, I. Ferreira, E. Fortunato, and R. Martins. "Design of optimized wave-optical spheroidal nanostructures for photonic-enhanced solar cells." In: Nano Energy 26 (2016), pp. 286 –296.

[61] S. Abdellatif, P. Sharifi, K. Kirah, R. Ghannam, A. Khalil, D. Erni, and F. Marlow. "Re-fractive index and scattering of porous TiO2 films." In: Microporous and Mesoporous Materials 264 (2018), pp. 84–91.

[62] J. Caram, N. Budini, and R. D. Arce. "Analysis of substrate coverage of hybrid halide perovskite thin films deposited on glass." In: Matéria (Rio de Janeiro) 23.2 (2018).

[63] T. Oku. "Crystal structures of CH3NH3PbI3 and related perovskite compounds used for solar cells." In: Solar Cells-New Approaches and Reviews 1 (2015).

[64] B. Cai, W.-H. Zhang, and J. Qiu. "Solvent engineering of spin-coating solutions for planar-structured high-efficiency perovskite solar cells." In: Chinese Journal of Catalysis 36.8 (2015), pp. 1183–1190.

[65] A. Mei, X. Li, L. Liu, Z. Ku, T. Liu, Y. Rong, M. Xu, M. Hu, J. Chen, Y. Yang, et al."A hole-conductor–free, fully printable mesoscopic perovskite solar cell with high stability." In: Science 345.6194 (2014), pp. 295–298.

[66] M. Jung, Y. C. Kim, N. J. Jeon, W. S. Yang, J. Seo, J. H. Noh, and S. Il Seok. "Thermal Stability of CuSCN Hole Conductor-Based Perovskite Solar Cells." In: ChemSusChem 9.18 (2016), pp. 2592–2596.

[67] B. N. Ezealigo, A. C. Nwanya, A. Simo, R Bucher, R. U. Osuji, M. Maaza, M. Reddy,and F. I. Ezema. "A study on solution deposited CuSCN thin films: Structural,electrochemical, optical properties." In: Arabian Journal of Chemistry (2017).

[68] H. Zhang, M. Tao, B. Gao, W. Chen, Q. Li, Q. Xu, and S. Dong. "Preparation of CH3NH3PbI3 thin films with tens of micrometer scale at high temperature." In: Scientific Reports7 (2017).

[69] M. J. Brites, M. A. Barreiros, V. Corregidor, L. C. Alves, J. V. Pinto, M. J. Mendes, E.Fortunato, R. Martins, and J. Mascarenhas. "Ultrafast Low-Temperature Crystallization of Solar Cell Graded Formamidinium-Cesium Mixed-Cation Lead Mixed-Halide Perovskites Using a Reproducible Microwave-Based Process." In: ACS Applied Energy Materials 2.3 (2019), pp. 1844–1853.

[70] J. Song, R. Yang, Z. Yulong, M. Che, L. Zhu, X. Gu, and Y. Qiang. "Morphology modification of perovskite film by a simple post-treatment process in perovskite solar cell." In: Materials Science and Engineering: B217 (Mar. 2017), pp. 18–25

[71] K. Kara, D. A. Kara, C. Kırbıyık, M. Ersoz, O. Usluer, A. L. Briseno, and M. Kus."Solvent washing with toluene enhances efficiency and increases reproducibility in perovskite solar cells." In: RSC Adv.6 (32 2016), pp. 26606–26611.

[72] G. W. P. Adhyaksa et al. "Understanding losses in halide perovskite thin films." Doctoral dissertation. Universiteit van Amsterdam, 2018.

[73] Q. Xue, Z. Hu, C. Sun, Z. Chen, F. Huang, H.-L. Yip, and Y. Cao. "Metallohalide perovskite–polymer composite film for hybrid planar heterojunction solar cells." In: RSC Advances5.1 (2015), pp. 775–783.

[74] X. Tang. "Investigation on the material stability of metal-halide perovskite semiconductors." Doctoral dissertation. Jan. 2019.

[75] S. Chavhan, O. Miguel, H.-J. Grande, V. Gonzalez-Pedro, R. S. Sánchez, E. M. Barea,I. Mora-Seró, and R. Tena-Zaera. “Organo-metal halide perovskite-based solar cells with CuSCN as the inorganic hole selective contact.” In: J. Mater. Chem. A2 (2014), pp. 12754–12760

[76] J. Chen, Y. Xiong, Y. Rong, A. Mei, Y. Sheng, P. Jiang, Y. Hu, X. Li, and H. Han.“ Solvent Effect on the Hole-conductor-free Fully Printable Perovskite Solar Cells. ”In: Nano Energy27 (2016)

[77] M. J. Brites, M. A. Barreiros, V. Corregidor, L. C. Alves, V. Pinto, M. J. Mendes, & J. Mascarenhas (2019). Ultrafast Low-Temperature Crystallization of Solar Cell Graded Formamidinium-Cesium Mixed-Cation Lead Mixed-Halide Perovskites Using a Reproducible Microwave-Based Process. ACS Applied Energy Materials, 2(3), pp. 1844-1853.

[78] N. Arora, M. I. Dar, A. Hinderhofer, N. Pellet, F. Schreiber, S. M. Zakeeruddin, and M. Grätzel. “Perovskite solar cells with CuSCN hole extraction layers yield stabilized efficiencies greater than 20%.” In: Science 358.6364 (2017), pp. 768–771.

[79] Solar Cell I-V Characteristic: http://www.alternative-energy-tutorials.com/energy-articles/solar-cell-i-v-characteristic.html (Visited on 28/9/2019)

[80] M. Köntges, S. Kurtz, C. Packard, U. Jahn, K. Berger, C Buerhop, G. Razongles, and G. Friesen.” Review of Failures of Photovoltaic Modules Final” (2015)

Appendices

A. Solar Cell Parameters

In this section it is explained how to calculate the solar cell's parameters by analysing the I-V and P-V curves (Figure 30), obtained by the electrical characterization, and using the appropriate equations (presented below) to extract its values. It is also represented in Figure 31, the influence of the shunt and series resistances on the shape of the I-V curves and on the FF obtained.

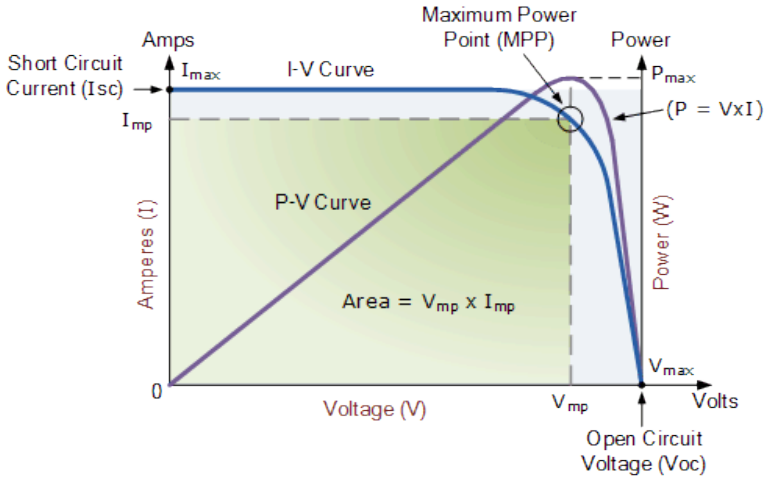

Figure 30 - Representation of the electrical parameters extraction of a solar cell from the I-V and P-V curves [79].

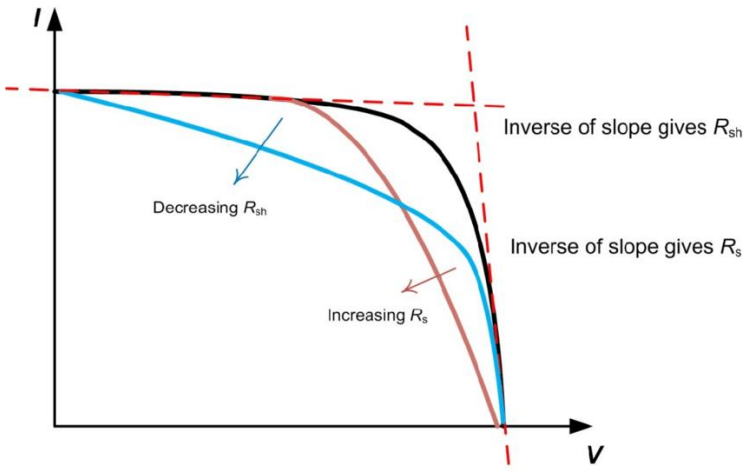

Figure 31 - Effect of varations of the series and shunt resistance (RS and RSH, respectively) in the I-V curve of a solar cell [80].

- I_{SC} (short circuit current) is the current value for V = 0 V;
- V_{OC} (open circuit voltage) is the voltage value for I = 0 V;
- The series resistance (Rs) and shunt resistance (Rsh) values are obtained by calculating the inverse of the IV curves slope, as shown in Figure 31. It is desirable that the R_s is as low as possible and the R_{SH} as high as possible.
- Imp and Vmp are the maximum current and voltage, respectively, and can be interpreted by analysing the IV curve, as illustrated in Figure 30;
- P_{max} (maximum power): $P_{max} = I_{mp} \, x \, V_{mp}$ (1)
- FF (fill factor), approximation of the IV curve to a square: $FF = \frac{Imp \, x \, Vmp}{Isc \, x \, Voc}$ (2)
- PCE (Power conversion efficiency), ratio between Pmax and Plight (light power = 1000 W/m^2): $FF = \frac{Pmax}{Plight} \, x \, 100\%$ (3)

B. Materials

Table 11 - List of reagents used for this work, with their respective abbreviation, purity, CAS and company.

Material	Abbreviation	Purity	CAS	Company
Absolute Ethanol	EtOH	99,99%	64-17-5	FISHER CHEMICAL
Transparent Titania (TiO_2) Paste	-	99%	-	SIGMA-ALDRICH
Copper (I) Thiocyanate	CuSCN	96%	1111-67-7	ALFA AESAR
Diethyl Sulfide	-	98%	352-93-2	SIGMA-ALDRICH
γ-Butyrolactone	GBL	99%	96-48-0	PANREAC
Hidrochloric Acid	HCl	37%	017-002-01	FLUKA
Lead Iodide	PbI_2	99%	10101-63-0	SIGMA-ALDRICH
Lithium Salt	Li-TFSI	99,95%	90076-65-6	SIGMA-ALDRICH
Methylammonium Iodide	MAI	98%	14965-49-2	SIGMA-ALDRICH
Titanium (IV) Isopropoxide	TTIP	97%	546-68-9	SIGMA-ALDRICH
Toluene	-	99.8%	108-88-3	FISHER CHEMICAL
Zinc Powder	-	99.9%	9029-97-4	SIGMA-ALDRICH

C. Solutions Preparation

In this section it is described the recipes and preparation methods of some solutions referred in the experimental section.

1. ETL

The compact TiO_2 (c.TiO_2) solution was prepared by mixing two different solutions. One solution, composed of 18 µL of hydrochloric acid (HCL) in 1.25 mL of absolute ethanol (EtOH), was dropwise to a solution of 180 µL of titanium (IV) isopropoxide (TTPI) in 1.25 mL of absolute ethanol (EtOH), after both solutions had been stirring for around 30 min.

The mesoporous TiO_2 (mp.TiO_2) was prepared by dissolving 120 mg of titania paste (Sigma-Aldrich) in 1 mL of absolute ethanol (EtOH).

2. Perovskite Solutions

The perovskite solutions were produced by dissolving lead iodide (PbI_2) and methylammonium iodide (MAI) in γ-butyrolactone (GBL), with different concentrations (0.8 M, 1 M and 1.2 M).

For the 1 M perovskite solution, 461 mg of PbI_2 and 159 mg of MAI were dissolved in 1 mL of GBL and were left stirring at 65 ºC.

D. Optical Characterization

In this section, the Tauc plots used to obtain the band gap values of some produced cells studied in this work, are shown in Figure 32. Also, in Figure 33 it is studied the optical performance of two solar cells with two different CuSCN deposition methods.

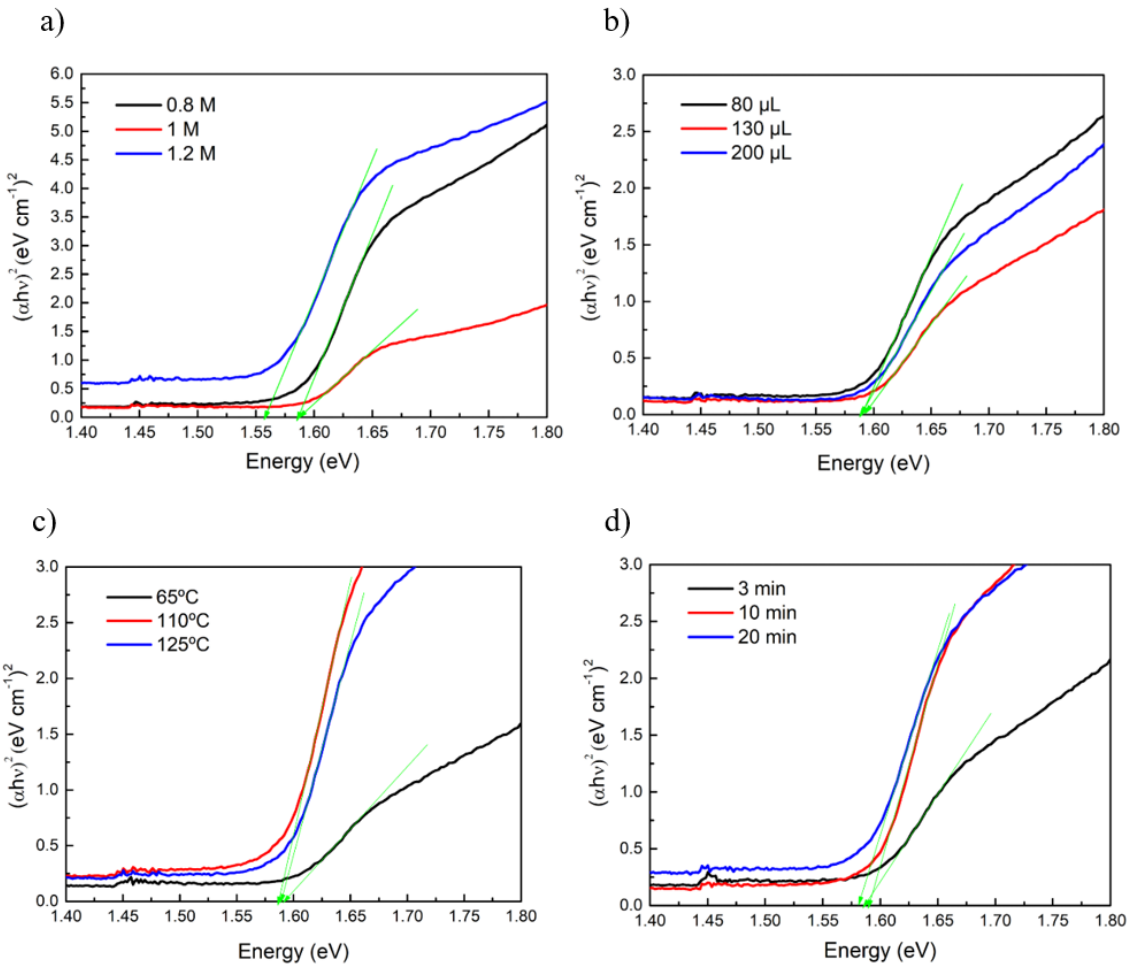

Figure 32 - Tauc plots with indication (arrows) of the band gap of each cell studied for the parameters: a) Perovskite solution concentration; b) Toluene washing volume; c) Perovskite layer annealing temperature; d) Perovskite layer annealing time.

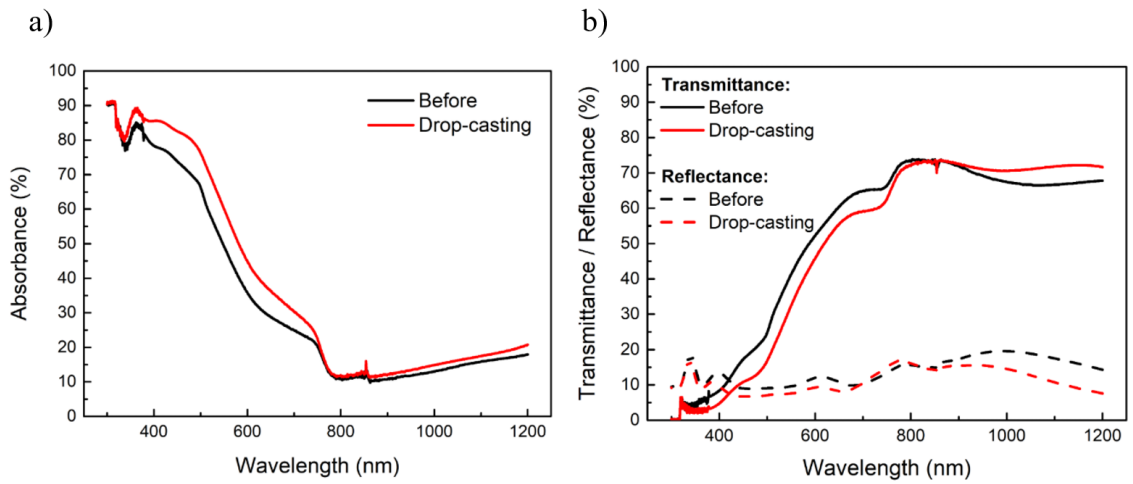

Figure 33 - a) Absorbance, b) Transmittance and reflectance spectra of two samples, one on which the CuSCN deposition was done during the spinning by drop-casting method (red) and other on which the CuSCN deposition was performed before the spinning started (black).

E. Opto-electronic Characterization

This section shows the J-V and P-V curves from the CuSCN deposition study, which compares the electrical performance between a cell on which CuSCN was deposited by drop-casting and other one on which the CuSCN was deposited before the spinning started.

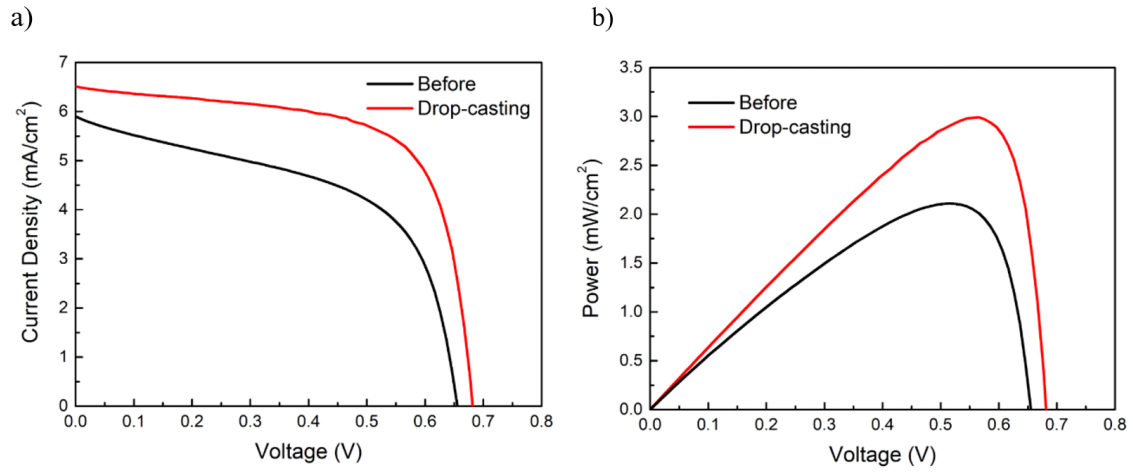

Figure 34 - a) J-V and b) P-V curves extracted from the electrical characterization results of two cells on which were performed different CuSCN depostion methods: CuSCN deposited before the spinning started (black) and drop-casting while the substrate was already spinning (red).